Organic & Biomolecular Chemistry

PAPER

View Article Online
View Journal | View Issue

Cite this: *Org. Biomol. Chem.*, 2014, **12**, 2686

Bio-inspired benzo[*k*,*l*]xanthene lignans: synthesis, DNA-interaction and antiproliferative properties†

Carmela Spatafora,[a] Vincenza Barresi,[b] Vedamurthy M. Bhusainahalli,‡[a] Simone Di Micco,[c] Nicolò Musso,[b] Raffaele Riccio,[c] Giuseppe Bifulco,[c] Daniele Condorelli[b] and Corrado Tringali*[a]

Received 17th December 2013,
Accepted 21st February 2014

DOI: 10.1039/c3ob42521e

www.rsc.org/obc

In this work twelve benzo[*k*,*l*]xanthene lignans were synthesized by biomimetic, Mn-mediated oxidative coupling of caffeic esters and amides. These compounds, bearing different flexible pendants at position C1/C2 of the aromatic core, interact with DNA in a dual mode, as confirmed by DF-STD NMR analysis and molecular docking: the planar core acts as a base pair intercalant, whereas the flexible pendants act as minor groove binders. Their antiproliferative activity was evaluated on a panel of six tumor cell lines: HT-29, Caco-2, HCT-116 (human colon carcinoma), H226, A549 (human lung carcinoma), and SH-SY5Y (human neuroblastoma). All compounds under study, except **29**, resulted in activity against one or more cell lines, and the markedly lipophilic esters **13** and **28** showed the highest activity. Compound **13** was more active than the anticancer drug 5-fluorouracil (5-FU) towards HCT-116 (colon, GI_{50} = 3.16 μM) and H226 (lung, GI_{50} = 4.33 μM) cell lines.

Introduction

Renewed attention to natural or nature-derived bioactive compounds as lead compounds in drug discovery has been observed in recent years.[1] This trend is probably connected with the observation that the significant decrease in the number of new molecular entities (NMEs) drugs approved by the U.S. Food and Drug Administration over the period 1990–2010 might be related to the reduced attention to natural products as sources of new therapeutic leads towards the end of 20th century.[2] Moreover, many anticancer drugs available today have been developed from natural leads,[3] and a number of new anticancer candidates derived from natural products are currently in Phase II or Phase III clinical trials.[4] Thus, many families of natural products have been investigated in an effort to discover or develop new bio-inspired antitumor agents, and hundreds of promising synthetic analogues have been obtained. Many of these studies refer to lignans and related compounds, well-known for their large structural variety and for including examples of highly bioactive compounds, the most famous being podophyllotoxin (**1**, Fig. 1) whose optimization has afforded the anticancer drugs etoposide (**2**), etopophos (**3**) and teniposide (**4**).[5]

Dimeric lignans are biosynthetically originated by coupling of two phenylpropanoid (C_6C_3) units, and a number of lignans and analogues have been synthesized by biomimetic oxidative coupling;[6] among these, benzo[*k*,*l*]xanthene lignans (in the following, more briefly 'benzoxanthene lignans') have recently been made available by some of us through a simple biomimetic methodology,[7] in the frame of our studies on nature-derived compounds as potential antitumor agents.[8] The oxidative coupling of caffeic esters allowed us to obtain in good yields both natural and 'unnatural' lignans with a planar and intensively fluorescent benzo[*k*,*l*]xanthene core, very rarely found in nature. To the best of our knowledge, to date only five natural benzoxanthene lignans have been reported in the literature, namely rufescidride (**5**) from *Cordia rufescens*[9] and *Taraxacum mongolicum*,[10] mongolicumin A (**6**) from *T. mongolicum*,[10] yunnaneic acid H (**7**) from *Salvia yunnanensis*,[11] chiliantin D (**8**) from *Rhoiptelea chiliantha*[12] and dodegranoside C (**9**) from *Dodecadenia grandiflora*.[13] By biomimetic dimerization of methyl caffeate (**10**) and CAPE (Caffeic Acid Phenethyl Ester, **11**), the latter being an anti-inflammatory, antioxidant and antiproliferative component of propolis,[14] we have firstly obtained, respectively, the synthetic benzoxanthenes **12** and **13**; also the natural benzoxanthenes **5**, **6** were synthesized. We have proposed a probable mechanism of formation of these

[a]*Dipartimento di Scienze Chimiche, Università degli Studi di Catania, Viale A. Doria 6, I-95125 Catania, Italy. E-mail: ctringali@unict.it*
[b]*Dipartimento di Scienze Bio-Mediche, sezione di Biochimica, Università degli Studi di Catania, Viale A. Doria 6, I-95125 Catania, Italy*
[c]*Dipartimento di Farmacia, Università di Salerno, via Giovanni Paolo II, 132, 84084 Fisciano (SA), Italy*
†Electronic supplementary information (ESI) available. See DOI: 10.1039/c3ob42521e
‡Present address: Department of Inorganic and Physical Chemistry, Indian Institute of Science, CV Raman Road, Bangalore, Karnataka 560012, India.

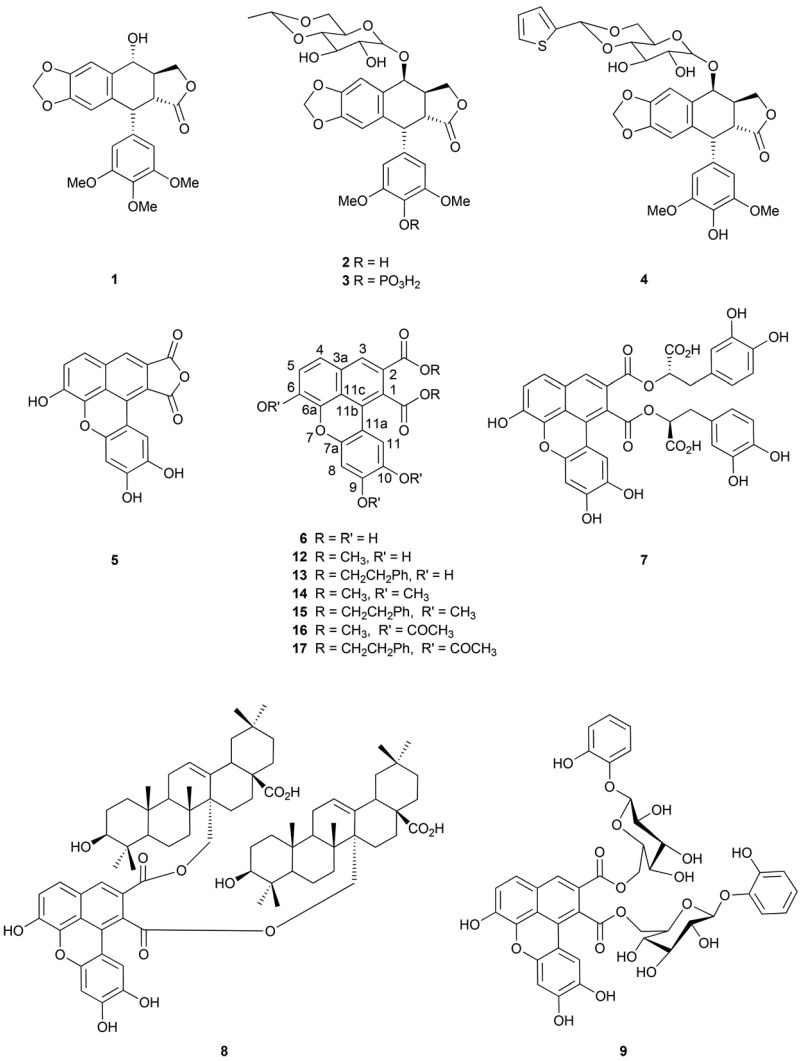

Fig. 1 Structures of compounds **1–9** and **12–17**.

compounds (corroborated by calculations) by a β–β′ (8–8′) oxidative coupling of two caffeoyl residues.

The lack of biological data on benzoxanthene lignans, as well as their planar and extensively conjugated nucleus, prompted us to study their DNA-interaction and antiproliferative properties: to establish the role of the hydroxyl groups in C-6, C-9 and C-10 and define some structure–activity relationships, we prepared the permethyl derivatives **14** and **15** and the peracetyl derivatives **16** and **17**. These were evaluated, together with **5**, **12** and **13**, both for their DNA interaction (studied by STD-NMR experiments and molecular docking) and for their antiproliferative activity towards SW480 (colon carcinoma) and HepG2 (hepatoblastoma) cancer cells.[15] The results of this study demonstrated that benzoxanthene lignans are able to interact with DNA in a dual mode: the planar core acts as a base pair intercalant, whereas the flexible pendants in C-1 and C-2 act as minor groove binders.

In particular, docking calculations revealed that the hydroxy groups in C-6, C-9 and C-10 are of crucial importance for intercalation, being involved in hydrogen bonds both with guanines and with the anomeric oxygen of deoxyribose, whereas the C-1/C-2 pendants are collocated along the grooves of the nucleic acid and make contact with the external deoxyribose/backbone. These results were in agreement with biological data: indeed, the benzoxanthene **13** (GI_{50} = 2.57 μM on SW480 cells), with the predicted higher affinity for the minor groove, proved significantly more active than **12** (GI_{50} = 4.76 μM on SW480 cells); the permethylated derivatives **14** and **15** were substantially inactive, indicating that the free hydroxyl groups are essential for the antiproliferative activity. Interestingly, the peracetates **16** and **17** were active, and docking calculations showed that the interactions of the benzoxanthene core with the macromolecular counterpart are realized through the change of hydrogen bond donors into acceptors. Rufescidride (**5**), lacking flexible pendants, also proved inactive and this confirmed the importance of the ester pendants for the antiproliferative activity of these compounds. It is also worth mentioning here that the CAPE-derived lignan **13** has recently been reported by some of us as an inhibitor of both new vessel growth in the angiogenesis bioassay and VEGF secretion.[16]

Compound **13** also inhibited colon adenocarcinoma (WiDr) cells more effectively than its analog **12**, showed DNA-damage and pro-apoptotic properties and induced autophagy in WiDr cells.[17] Very recently, we have also shown that compounds **12** and **13** react efficiently with peroxyl radicals in both polar and nonpolar solvents.[18] On the basis of these promising results, we decided to continue the study of 'bio-inspired' benzoxanthene lignans not only for their rarity in nature and consequent poor biological evaluation, but also for their dual-mode interaction with DNA. Anticancer agents that bind to DNA commonly act either by intercalation between base pairs or by minor groove binding; molecules able to establish a dual mode interaction with DNA have been less frequently reported and, in principle, should give stronger interaction with DNA and a potential inhibitory activity towards DNA processing enzymes;[19] to cite one example, combilexins are a promising group of DNA hybrid ligands having a minor groove binding element combined with an intercalating planar core. These hybrid molecules should be able to interact with DNA to a greater extent, interfering with DNA–protein interaction and resulting inhibitors of topoisomerase I and II.[20] Thus, we planned the synthesis of a new set of compounds bearing different pendants in order to implement the previous SAR data, in particular on the role of the flexible pendants and their minor groove binding interactions.

Bearing in mind the observed different antiproliferative activity of lignans **5**, **12** and **13**, we planned to evaluate and compare the effects of the following modifications of the C-1/C-2 pendants: (a) acyl residues of different dimensions, namely with a longer acyl chain or an aromatic ring, able to establish van der Waals interactions with the minor groove; (b) the presence of polar groups with donor or acceptor properties in the formation of hydrogen bonds; (c) isosteric substitution of the ester with amide functions: the latter might prove to be of some importance, because of the higher metabolic stability of the amides, if the compounds under study were degraded by intracellular esterase enzymes before reaching the biological target.

Thus, we report here the synthesis of new benzoxanthene lignans together with the study of their interaction with DNA through a differential frequency-saturation transfer difference (DF-STD) protocol,[21] based on STD-NMR experiments,[22] and by molecular docking calculations to study the three-dimensional complex of ligands and DNA; these compounds, in addition to the previously active ones **12** and **13**, were evaluated for their antiproliferative activity against six cell lines, namely HT-29, Caco-2, HCT-116 (human colon carcinoma), H226, A549 (human lung carcinoma), and SH-SY5Y (human neuroblastoma).

Results and discussion

Our previous work on the interaction of benzoxanthene lignans with DNA[15] established the importance of C-6, C-9 and C-10 hydroxy groups in stabilizing the intercalation between base pairs, and also suggested that the C-1/C-2 pendants have a significant role in minor groove binding. In this work we focused our study on these pendants and report in the following the synthesis of new benzoxanthene lignans, the experimental measurement of their interaction with DNA through DF-STD, the molecular docking study of these products with DNA, and the evaluation of their antiproliferative activity towards six tumor cell cultures, in comparison with the benzoxanthenes **12** and **13**, previously found active towards colon (SW480) and hepatic (HepG2) cancer cells.

Synthesis

The benzoxanthene lignans discussed here have been synthesized through a biomimetic methodology previously reported by some of us[7] and based on a Mn-mediated oxidative coupling. A series of caffeic acid derivatives, namely the esters **10**, **11** and **18–23**, as well as the amides **24–26** were subjected to the oxidative coupling reaction in the presence of $Mn(OAc)_3$, according to the general Scheme 1, and afforded the benzoxanthene lignans **12**, **13** and **27–36**.§

The coupling reactions of both methyl caffeate (**10**) and CAPE (**11**) to obtain the dimers **12** and **13** were carried out in chloroform as previously reported. Under analogous conditions, ethyl caffeate (**18**) and butyl caffeate (**19**), prepared by esterification of caffeic acid, afforded respectively the benzoxanthene diesters **27** and **28** as the main products; these were purified and characterized by spectral analysis. The signals in

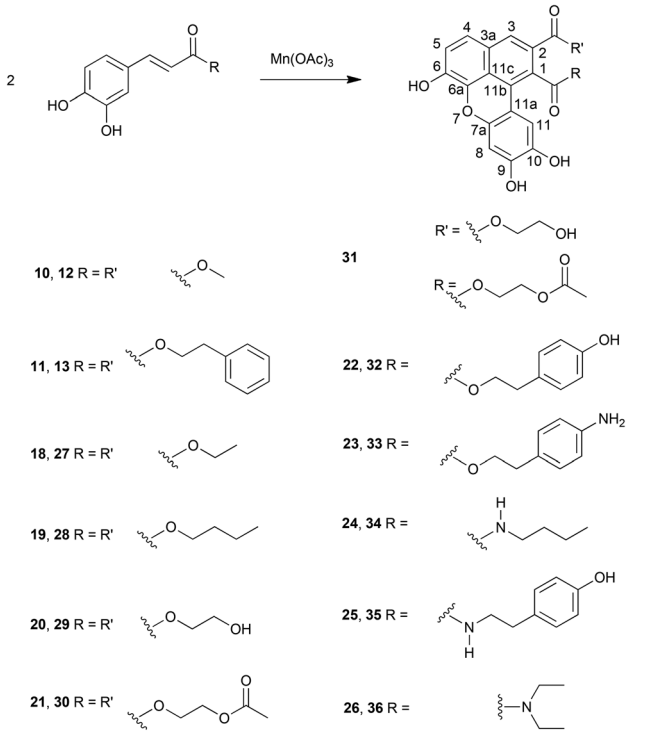

Scheme 1 Synthesis of compounds **12**, **13**, and **27–36**; the first number refers to the monomer, and the second to dimers.

§ All data concerning the reported compounds will be included in LIBIOMOL, the chemical library of natural and synthetic bioactive molecules, accessible at the website http://www.libiomol.unina.it

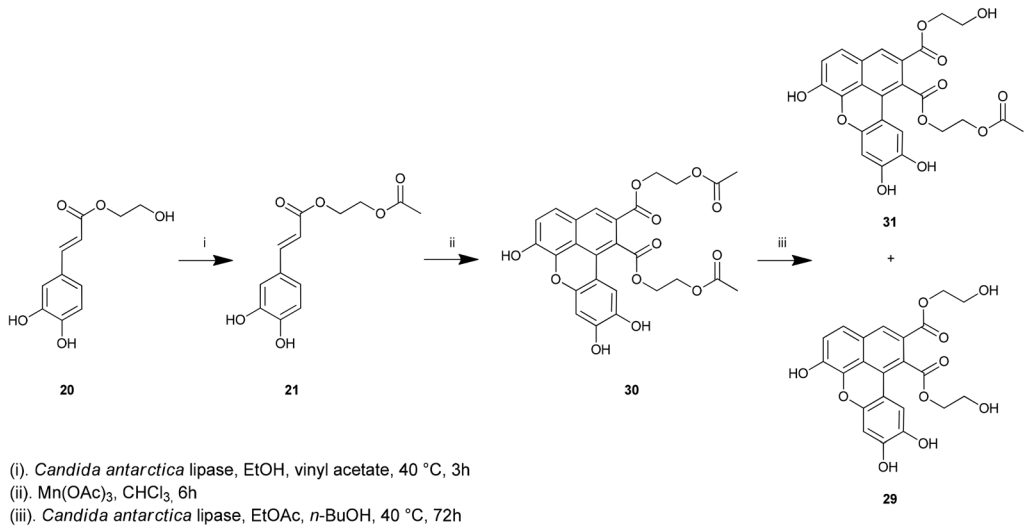

Scheme 2 Synthesis of compounds **29–31**.

their ^{1}H and ^{13}C NMR spectra were easily assigned by comparison with those of the related dimers **12** and **13**. In order to evaluate the effect of pendants with polar groups, caffeic acid was esterified with ethylene glycol to obtain the hydroxyethyl caffeate; the oxidative coupling of this substrate required the addition of ethanol to the reaction mixture, and this resulted in a lower yield of the dimer **29**, in agreement with the solvent effects reported in our previous study. We therefore turned to a chemo/regioselective enzymatic methodology, summarized in Scheme 2, which allowed obtaining not only the dimer **29** with higher yields, but also the diacetate **30** and the monoacetate **31**, useful to compare the effect of different groups in the pendant chain. Indeed, employing lipase from *Candida antarctica* (CaL) and vinyl acetate, we were able to initially obtain the acetoxyethyl caffeate **21**, and this substrate was effectively dimerized with $Mn(OAc)_3$ in chloroform to give **30** as the main product.

Subsequently, this dimer was submitted to an enzymatic alcoholysis with *n*-butanol in the presence of CaL; the enzyme removed preferentially the acetyl group from the C-2 chain, so in a first step the monoacetylated benzoxanthene **31** was obtained. By prolonging the reaction time to 72 h, the acetate at C-1 was also removed, and a mixture of compounds **29**, **30** and **31** was obtained. After prolonged extension of the reaction time, no further conversion of the starting material was observed. Compounds **29–31** were purified and a complete assignment of their ^{1}H and ^{13}C NMR spectra was carried out; an unambiguous assignment was achieved, when necessary, by analysis of two-dimensional NMR spectra, as exemplified in Fig. 2, reporting selected HMBC correlations for the signal assignments of the C1/C2 pendants in compound **31**.

A further dimer, **32**, was designed on the basis of our previous study, indicating **13** as the best DNA-interacting benzoxanthene lignan, and highlighting the strong binding of the two phenylethyl groups along the DNA minor groove. Thus, we planned a slight modification of this pendant by esterification of caffeic acid with the natural phenolic alcohol tyrosol (one of

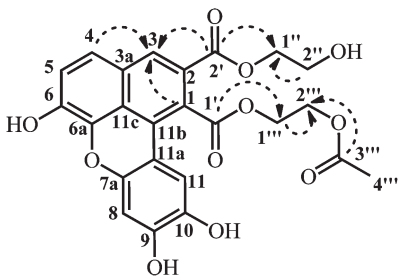

Fig. 2 Key HMBC correlations for the signal assignments of the C1/C2 pendants in compound **31**.

the phenolic components of olive oil),[23] to evaluate the effect of a *p*-hydroxy group on the aromatic ring, in comparison with the dimer derived from CAPE. The tyrosil caffeate **22**, obtained in the presence of DCC and DMAP, was subjected to the coupling reaction with $Mn(OAc)_3$ in a chloroform–ethanol mixture, and afforded **32** as the main product. As a variation of this model, we carried out the synthesis of a similar ester employing, instead of tyrosol, the 2-(4-aminophenyl)ethanol, in order to have pendants with a *p*-amino group on the aromatic ring. The 4-aminophenethyl caffeate **23**, prepared analogously to **22**, was dimerized with $Mn(OAc)_3$ in chloroform–ethanol, and the diester **33** was the main product.

In addition to the above cited benzoxanthene esters, we carried out the synthesis of some benzoxanthene amides; as a matter of fact, it is well known that amides have a higher metabolic stability than esters, the latter frequently being substrates for intracellular esterases. Consequently, amides could be more active than the corresponding esters because of the greater probability of reaching the biological target without chemical modifications. Hence we prepared the primary amides **24** and **25**, isosteric respectively with the esters **19** and **22**; a further amide **26** was prepared to test the effect of a more crowded *N*,*N*-disubstituted amide on both minor groove

binding and antiproliferative activity. These amides were synthesized from caffeic acid employing BOP/Et_3N; the dimerization reactions were carried out in ethanol and afforded respectively the benzoxanthene diamides **34**, **35** and **36** as the main products, although with lower yields with respect to the diesters. Also these further benzoxanthenes were subjected to a complete NMR study to confirm the structure and assign ^1H and ^{13}C NMR spectra.

DF-STD analysis

In order to detect the interaction of compounds **27–36** with the DNA and to understand their binding mode, the DF-STD method[21] was carried out by using a poly(dG–dC)·poly(dG–dC) copolymer as a macromolecule. This method is based on the acquisition of two STD-NMR[22] experiments at two different saturation frequencies,[21] and it allows distinguishing the binding mode of DNA ligands (minor groove binders, intercalators, external binders). Analogously to our previous DF-STD investigation of benzoxanthene lignans with DNA,[15] two distinct binding mode indexes (BMI, Table 1) were calculated for compounds **27–36** (see the Experimental section): the BMI, relative to the polycyclic aromatic core, and the BMI′, referred to the chemical appendages in positions C-1 and C-2 of the benzoxanthene core. This strategy was also adopted for the doxorubicin in our original contribution on DF-STD,[21] and was recently reported by Gomez-Monterrey *et al.* for the analysis of DNA-interacting spiro derivatives.[24] The BMI is a numerical parameter that, taking into account the relative intensities of STD effects at different saturation frequencies, gives insights on binding contacts of the ligands on the DNA surface.[21] The experimental DF-STD results showed that all compounds **27–36** interacted with the macromolecule (Fig. 45S–53S†), as exemplified in Fig. 3 for compound **35**.

In particular, the results of the DF-STD analysis confirmed that the polycyclic aromatic portion intercalates between the base pairs of the nucleic acid (BMI values, Table 1), whereas the flexible pendants at C-1 and C-2 are placed in the minor groove (BMI′ values, Table 1). These data are in agreement

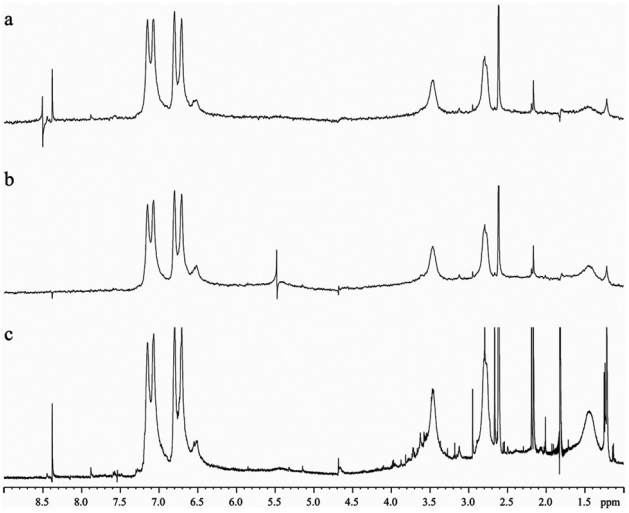

Fig. 3 DF-STD spectra of the **35**–DNA complex. (a, b) STD spectra recorded upon saturation in the aromatic (8.5 ppm) and deoxyribose/backbone (5.0 ppm) spectral regions, respectively. (c) Reference STD spectrum with off-resonance irradiation (–16 ppm).

with our previous outcomes obtained from the interactions of **12**, **13** and other benzoxanthene lignans with the poly(dG–dC)·poly(dG–dC) copolymer.[15] In Table 1, the BMI and BMI′ values previously obtained for **12** and **13** have been added to aid structure–activity relationship considerations.

The BMI values of **27–36** show that the planar core establishes extended van der Waals contacts with the base pair aromatic rings and is also involved in interactions with the DNA backbone. Indeed, the obtained BMI values (ranging from 0.7 to 1.1) are clearly in line with data reported for unusual DNA intercalators such as ethidium bromide (BMI = 0.9)[21] which interacts with external negatively charged phosphate by its amino groups. Moreover, these values agree with the BMI of 0.9 obtained by us for rufescidride (**5**),[15] the above cited natural benzoxanthene anhydride with the same polyaromatic portion of **27–36** but lacking flexible pendants. The DF-STD data suggest that the hydroxyl groups in C-6, C-9 and C-10 of the planar moiety could be involved in hydrogen bonds with the deoxyribose/backbone of the nucleic acid. The observed differences in BMI values for compounds sharing the same polyaromatic core suggest that the substituents at C-1 and C-2 have an influence on the interaction with the macromolecule by determining different contact distances. The BMI′ values obtained for compounds **27–36** show that the 1,2 substituents are accommodated along the minor groove of the macromolecule. In particular, the BMI′ values of **27**, **28**, **30**, **32**, **33** and **35** (ranging from 0.5 to 0.8) highlight a comparable saturation diffusion irradiating on the aromatic and aliphatic DNA resonances. They are consistent not only with our previous data obtained for benzoxanthenes **12** and **13** but also with similar values obtained for well-known minor groove binders, such as distamycin A (BMI = 1.1) and netropsin (BMI = 0.9).[21] The BMI′ are also in agreement with the experimental data describing the interaction of distamycin A with the minor

Table 1 Binding mode index values for compounds **12**, **13** and **27–36** calculated by eqn (1)

Compound	BMI[a]	BMI′[a]
12[b]	1.2	0.7
13[b]	1.4	0.8
27	0.7	0.6
28	0.7	0.7
29	0.7	0.3
30	0.9	0.7
31	0.7	0.4
32	1.1	0.5
33	0.9	0.8
34	0.7	0.4
35	0.8	0.8
36	0.9	0.4

[a] Signal-to-noise ratios have been calculated integrating 4 empty regions in the spectra, finding a maximum error of 8%. [b] Values for **12** and **13** are reported from our previous work.[15]

groove of a DNA quadruplex (BMI = 0.8).[25] The BMI′ values obtained for **29**, **31**, **34** and **36** suggest a much closer contact with the deoxyribose/backbone than the base pairs of the biological target. Taken as a whole, the DF-STD data clearly indicate that the different structures of the various flexible substituents at C-1, C-2 influence the overall interaction contact with the DNA.

Molecular docking studies

Along with STD NMR experiments, we performed molecular docking calculations to acquire/produce a 3D model of the complex between compounds **27–36** and the DNA, and to shed light on the structure–activity relationships of these benzoxanthene lignans, in particular for the possible role of the flexible pendants at C-1 and C-2. As previously described for compounds **12** and **13**, two binding sites were considered (Fig. 4) for the investigation of base pair intercalation to understand if the stacking into the DNA and the hydrogen bond formation were base-dependent.

The analysis of docking calculations confirmed that lignans **27–36** intercalate between the base pairs of the DNA by their planar core and located the flexible appendages at different points of the DNA surface (Fig. 5), in accord with the findings obtained by the experimental DF-STD data.

Concerning the analysis of the interactions with Model A, the polycyclic aromatic moiety of **27–36** presents the same orientation between the base pairs of the DNA (Fig. 5a). In particular, the hydroxyl group in C-10 of **27–36** donates hydrogen bonds both to the anomeric and 5′ oxygen of **C13** (Fig. 5a), with atom distance ranges respectively of 1.76–2.30 Å and 2.32–2.75 Å. The different lengths and angles of the hydrogen bonds are dependent on the different chemical structures of the substituents in C-1 and C-2. These outcomes are in line with the above reported experimental BMI values (Table 1). Moreover, compound **30** donates a hydrogen bond by the OH in C-9 to N-7 of **G3**. This interaction could potentially be made also by the other compounds thanks to the rotation of the hydroxyl group. The flexible pendants are located along the minor groove of the DNA, in agreement with the experimentally determined BMI′ data (Table 1), and contribute to the complex stability by hydrogen bonds and hydrophobic interactions. The ester oxygen in C-1 accepts a H-bond from the NH_2 group of **G14** (Fig. 6a). Concerning the oxygen in C-2, we observed the same interaction with N-7 of **G3** by only **29** and **33**. Compounds **12**, **13**, **27**, **28**, **30–32**, **34–36** were not involved in interaction with N-7 of **G3**, due to the structural features of the flexible substituents. The chemical switch of the ester into amide entails the conversion of the hydrogen bond acceptor into a donor with loss of interaction with the macromolecular counterparts. Indeed, **34–36** were not hydrogen bonded by their amide groups to the aromatic base pairs along the minor groove of the DNA (Fig. 6). Behind the

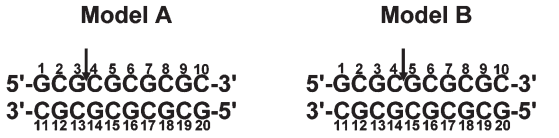

Fig. 4 Schematic representation of DNA Models (A and B) used in docking calculations. The sequence and numbering of two 10mers (A and B) DNA duplexes are reported. The arrows indicate the intercalation points.

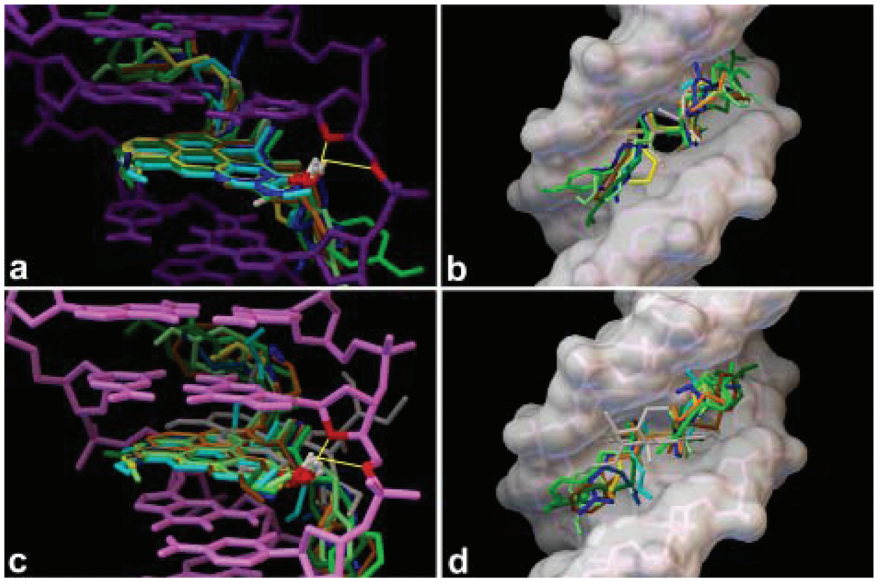

Fig. 5 Superimposition in the binding site of Models A (a, b purple) and B (c, d pink) of **12**, **13** and **27–36**. The ligands and DNA are represented by tube (a–d). In b and d, the macromolecule is also depicted by molecular surface. The ligands are coloured: **12**, lime; **13**, brown; **27**, grey; **28**, yellow; **29**, light blue; **30**, dark blue; **31**, blue; **32**, green; **33**, dark green; **34**, orange; **35**, light green; **36**, light grey. The OH in position 10 of **12**, **13**, **27–36**, and the anomeric and 5′ oxygen of **C13** (a) and **G14** (b) are coloured by atom type: polar H, white; O, red. The yellow line indicates hydrogen bonds. The figure highlights the overlapping binding modes of **12**, **13**, **27–36** in the binding site of Models A and B.

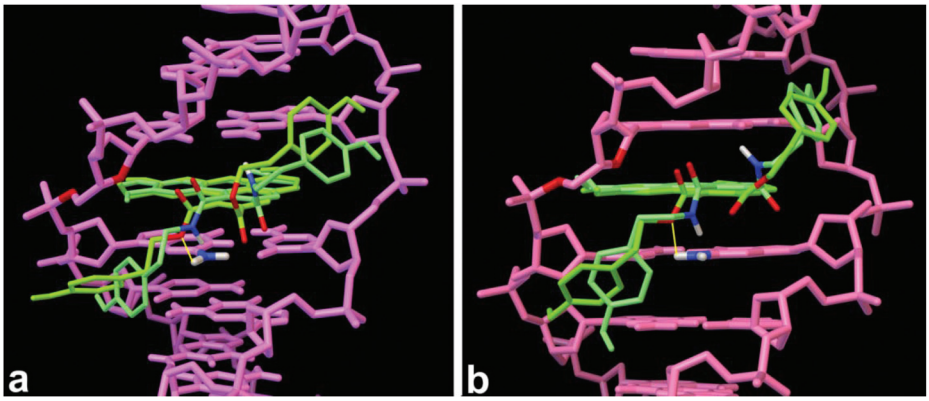

Fig. 6 Superimposition in the binding site of Models A (a, purple) and B (b, pink) of **32** and **35**. The ligands and DNA are represented by tube. The ligands are coloured: **32**, green; **35**, light green. The ester and amide groups in positions 1 and 2, and the NH_2 of **G14** (a) and **G5** (b) are coloured by atom type: polar H, white; O, red; N, sky blue. Yellow lines indicate hydrogen bonds. The figure is an example of the loss of a hydrogen bond by the amide group (**35**), compared to the ester functionality (**32**) along the minor groove of Models A (a) and B (b).

hydrogen bond formation, the substituents in C-1 and C-2 positions contribute to the DNA binding by hydrophobic interactions thanks to their carbon chains. In particular, as previously observed for compound **13**, the phenylethyl groups of **32**, **33** and **35** contribute more efficiently to the complex stability, giving wider van der Waals contacts along the minor groove of the DNA, compared to those lacking in the phenethyl groups (**27–31**, **34** and **36**).

Moreover, compounds **29–33** and **35** bear different chemical groups at the end of the carbon chain, such as OH, NH_2, $COCH_3$, which are hydrogen bond donors and acceptors. Indeed, these chemical functionalities are involved in interactions with macromolecular counterparts, further contributing to the binding towards the nucleic acid. In particular, **29** by the two hydroxy groups of its appendages donates hydrogen bonds to N-7 of **G3** and **G13**; **30** interacts with the same nucleotides found for **29**, accepting H-bonds by the CO of its acetate groups. Compound **31** accepts a H-bond from NH_2 of **G5** by its acetate on the appendage, and donates a H-bond by its OH to the oxygen 3′ of **G12**. The binders **32** and **35** donate H-bonds to the anomeric and 3′ oxygen of **G14**; these compounds, by the other OH of their appendages, donate a hydrogen bond to the oxygen in 3′ of **G3**. Compound **33** donates hydrogen bonds to CO in 2 and the oxygen 3′ of **C6**, by its NH_2 of the chemical arm bound to C-1. The other NH_2 donates hydrogen bonds to the anomeric oxygen of **G3** and to N-7 of **G12**.

Comparable findings are obtained by docking calculations on Model B. Indeed, the predicted bioactive conformations are similar, giving the same number of hydrogen bonds with comparable distances (Fig. 5b). The common planar moiety forms π–π interactions with base pairs of Model B (Fig. 5b), and the two pendants (in C-1 and C-2) are located in the minor groove establishing van der Waals contacts and hydrogen bonds (Fig. 5b). It is noteworthy that, besides the π-stacking, the planar portions of compounds **27–36** have the same orientation between two adjacent base pairs both in Model A and B (Fig. 5). With Model B, the OH in C-10 of **27–36** donates to both the anomeric (1.64–2.58 Å) and 5′ oxygen (2.03–3.14 Å) of **G14**, instead of **C13** with Model A (Fig. 5). These theoretical results are in agreement with the experimental BMI values reported in Table 1. Moreover, in our proposed 3D model the compounds **29**, **30** and **33** donate a hydrogen bond to N-7 of **G14** by their OH in C-9. The same interaction can potentially be made by **27–29**, **31–33**, **35** and **36**. As found for docked small molecules in Model A, compounds **29–33** and **35** accept and donate hydrogen bonds to and from DNA residues by the chemical appendages in positions C-1 and C-2. As reported above for Model A, the two hydroxy groups of **29** donate hydrogen bonds to N-7 of **G14** and the anomeric oxygen of **C6** and **C13**. Compound **30** accepts a H-bond from NH_2 of **G3** and **G5** by its CO of acetyl groups. The oxygen of the acetate at the end of the C-2 substituent accepts a hydrogen bond from NH_2 of **G14**. The binder **31** donates a hydrogen bond to N-7 of **G14** by its hydroxyl group, and accepts a H-bond by its CO of the acetate from NH_2 of **G5**. Compound **32** donates hydrogen bonds to the anomeric and 3′ oxygens of **C15** and **G12**, by the hydroxyl group of the substituents in C1 and C-2, respectively. By the NH_2 of the chemical arm bound to C-2, compound **33** donates a H-bond to CO in 2 of **C4** and accepts a H-bond from NH_2 of **G3**. The other amine group donates a H-bond to the anomeric oxygen of **C14**. By the OH of the C-2 appendage, the binder **35** donates a H-bond to CO in 2 of **C4** and accepts a H-bond from NH_2 of **G3**. The other hydroxyl group donates a hydrogen bond to the anomeric oxygen of **G7** and accepts a hydrogen bond from the NH_2 of **G16**.

Lipophilicity measurements

To acquire information about the lipophilicity of the compounds under study, as a first attempt we tried to run log *P* measurements, employing the classical method based on *n*-octanol/water partition.[26] However, we realized that the majority of compounds do not give reliable results, probably due to their poor solubility both in *n*-octanol and water. We therefore turned to an alternative method based on an RP-HPLC measurement.[27] This method has been applied in several cases to compare the relative lipophilicity of bioactive

molecules.[28] Hence, we carried out a C-18 reverse-phase HPLC analysis of the compounds to be evaluated. In Fig. 7 we report a superimposition of their HPLC profiles, which provides an indication of their relative lipophilicity; below we list these compounds in the order of decreasing lipophilicity, indicating the pertinent capacity factor (k) value[27b] in brackets: **28** (4.25) ≈ **13** (4.21) > **27** (3.24) > **32** (3.01) > **12** (2.92) > **34** (2.83) ≈ **30** (2.82) > **36** (2.59) > **31** (2.47) > **35** (2.39) > **33** (2.31) > **29** (2.09).

Interestingly, calculated log P values (in brackets) are in the order: **13** (6.65) > **28** (5.75) > **32** (5.34) > **27** (3.71) > **33** (4.28) > **34** (3.66) = **35** (3.66) > **12** (2.69) > **30** (2.52) > **36** (2.32) > **31** (1.60) > **29** (0.69). Both data concur well in indicating a marked lipophilicity of compounds **13** and **28** (and **27** with minor agreement), compared to all other benzoxanthenes.

Antiproliferative activity

The benzoxanthene lignans **27–36**, in addition to the previously reported **12** and **13**, were evaluated for their antiproliferative activity against six human cancer cell lines, namely HT-29, Caco-2, HCT-116 (colon carcinoma), H226, A549 (lung carcinoma), SH-SY5Y (neuroblastoma), by means of the MTT bioassay. The results are summarized in Table 2 and presented as the concentration inhibiting the 50% cell growth (GI_{50}). 5-Fluorouracil (5-FU), one of the most effective anticancer drugs, was used as positive reference.

These data show that, with the exception of **29**, the tested compounds exhibit significant antiproliferative activity against at least one cell line, although highly diverse biological responses were observed for the different cell lines. Interestingly, the CAPE-derived lignan **13** is more active than 5-FU against HCT-116 (GI_{50} = 3.16 μM with respect to 5.81 μM) and H226 (GI_{50} = 4.33 μM with respect to 16.41 μM); it is also highly active against A549 and SH-SY5Y, with GI_{50} of 11.07 and 11.28 μM, respectively. Also compound **28** is more active than 5-FU against HCT-116 cells (GI_{50} = 4.22 μM). The GI_{50} values obtained for **13** are in good agreement with those reported in our previous study,[15] namely 2.57 μM and 4.76 μM towards SW480 (colon carcinoma) and HepG2 (hepatoblastoma) cells, respectively, and confirm the promising antiproliferative activity of this compound. It has to be highlighted that

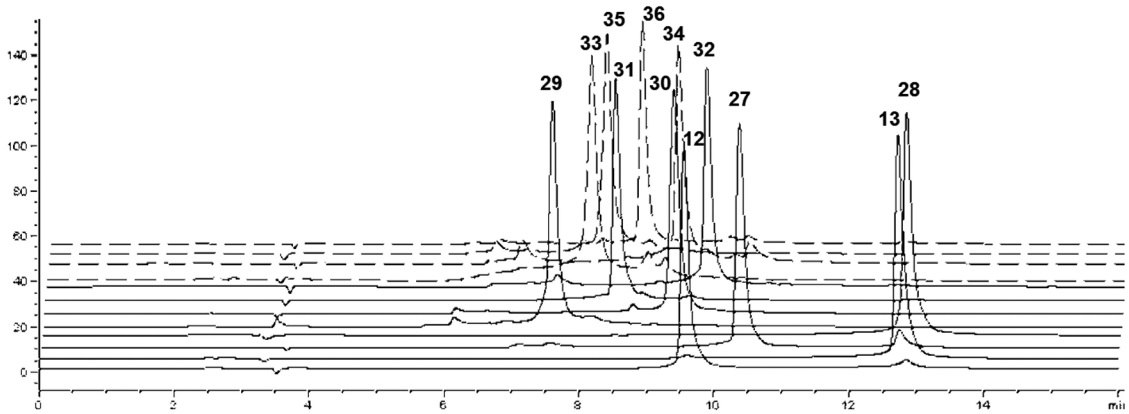

Fig. 7 Stacked plot of RP-HPLC-UV for compounds **12**, **13** and **27–36**. Note: a minimal shift to the right has been applied progressively from the lower to the higher profile.

Table 2 Antiproliferative activity of compounds **12**, **13**, and **27–36**

	GI_{50} (μM) ± SD*					
Compound	HT29[a]	Caco-2[b]	HCT-116[c]	H226[d]	A549[e]	SH-SY5Y[f]
12	100.00 ± 6.28	106.08 ± 13.47	31.46 ± 0.62	21.23 ± 0.15	35.50 ± 2.10	23.18 ± 2.03
13	27.38 ± 1.45	8.32 ± 0.67	**3.16 ± 0.38**	**4.33 ± 0.32**	11.07 ± 0.70	11.28 ± 0.93
27	80.20 ± 4.61	33.27 ± 1.37	32.41 ± 1.97	71.43 ± 4.88	68.28 ± 6.31	**3.56 ± 0.41**
28	35.41 ± 2.43	14.22 ± 1.49	**4.22 ± 0.15**	23.17 ± 1.27	33.18 ± 2.57	35.22 ± 3.21
29	>100	>100	>100	>100	>100	>100
30	>100	30.98 ± 1.45	63.32 ± 2.51	>100	>100	>100
31	>100	41.11 ± 2.19	>100	>100	>100	>100
32	31.12 ± 1.71	46.21 ± 1.91	26.72 ± 1.41	>100	>100	>100
33	>100	47.25 ± 4.12	>100	>100	>100	>100
34	>100	35.27 ± 3.19	>100	73.55 ± 4.81	>100	82.61 ± 7.57
35	>100	>100	>100	>100	>100	48.21 ± 3.93
36	>100	>100	>100	31.51 ± 2.51	38.43 ± 3.49	27.41 ± 2.31
5-FU	8.09 ± 0.51	**1.11 ± 0.05**	5.81 ± 0.31	16.41 ± 0.91	9.01 ± 0.51	**1.51 ± 0.11**

*GI_{50} (concentration causing 50% cell growth inhibition) calculated after 72 h of continuous exposure relative to untreated controls. Values are the means (±SD) of four experiments. Values lower than 5 μM are given in bold. [a] HT29: colon. [b] Caco-2: colon. [c] HCT-116: colon. [d] H226: lung. [e] A549: lung. [f] SH-SY5Y neuroblastoma.

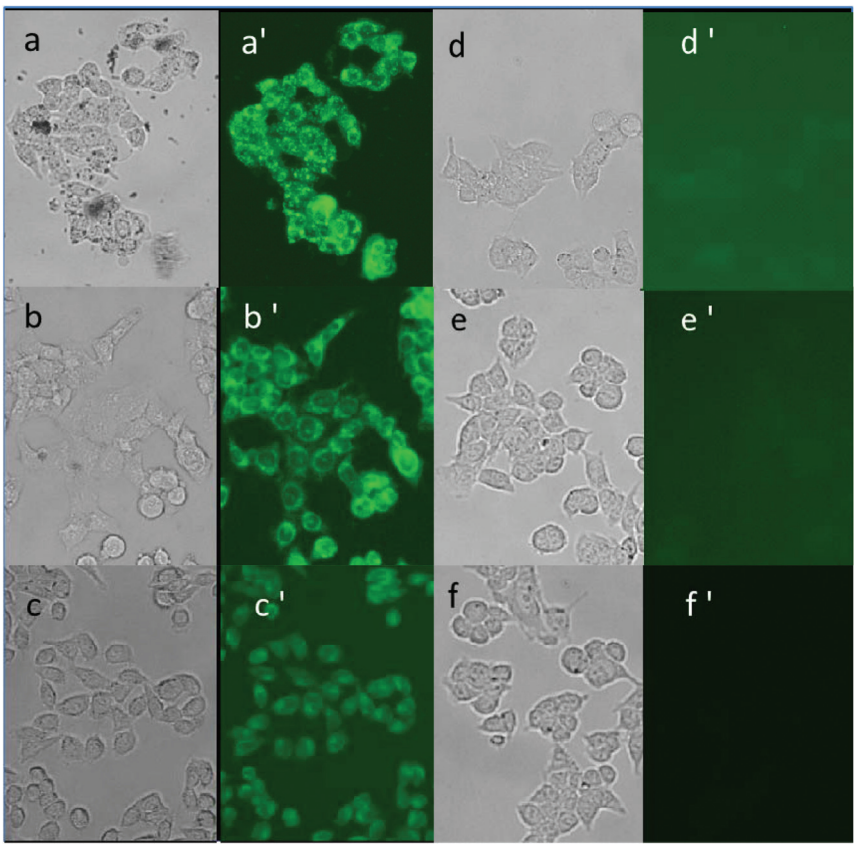

Fig. 8 (a, a′) Compound **13**; (b, b′) compound **28**; (c, c′) compound **32**; (d, d′) compound **34**; (e, e′) compound **35**; (f, f′) no treatment. (a–f): Phase contrast image; (a′–f′): fluorescence microscope image (excitation 345 nm; emission 455 nm). Cells were incubated with the indicated compounds for 15 min before taking the microphotographs except for compounds **34** and **35** whose incubation lasted for 1 hour to show the lack of staining even after prolonged treatment.

compound **27** showed high selectivity and was more active towards SH-SY5Y cells (GI_{50} = 3.56 μM).

It is noteworthy that by microscopic observation some compounds show a net fluorescence inside the cell, clearly indicating an effective uptake by the tumor cells. In particular, as shown in Fig. 8 with reference to the cell line HTC-116, this marked fluorescence was observed for the most potent and markedly lipophilic benzoxanthenes **13** and **28** (Fig. 8a′–b′), whereas a weaker fluorescence was observed for less potent compounds such as **32** (Fig. 8c′) or no significant fluorescence above the background could be observed for inactive compounds such as **35** (Fig. 7e′). Also interesting is the comparison between the esters **28** and **32** (Fig. 8b′–c′), showing a discernible fluorescence, and the structurally related, although less lipophilic, amides **34** and **35** (Fig. 8e′–d′) where no significant fluorescence could be observed.

Conclusions

In this work, we have extended our previous study on a rare group of natural and 'unnatural' lignans, obtained by biomimetic oxidative coupling of caffeic esters and possessing a planar and intensively fluorescent benzo[*k*,*l*]xanthene core. Analogously to the previously evaluated lignans **12** and **13**, the compounds **27–36** now examined were obtained by a biomimetic, Mn-mediated oxidative coupling; caffeic amides were also used in this study in addition to esters. These compounds, bearing different flexible pendants at position C1/C2 of the aromatic core, were subjected to a DF-STD NMR analysis, as well as to molecular docking calculations; these studies confirmed that all benzoxanthene lignans interact with DNA in a dual mode: the planar core acts as a base pair intercalant, whereas the flexible pendants act as minor groove binders; the reported data also showed that the structure of the pendant may affect the interaction with DNA. In particular, the diamides **34–36** lack a hydrogen bonding interaction with the aromatic base pairs along the minor groove of the DNA, observed for the diesters. A panel of six human cancer cell cultures, namely HT-29, Caco-2, HCT-116 (colon carcinoma), H226, A549 (lung carcinoma), and SH-SY5Y (neuroblastoma), was used to evaluate the antiproliferative activity of compounds **27–36** with those of **12** and **13**, previously showing antiproliferative activity towards SW480 (colon carcinoma) and HepG2 (hepatoblastoma) cancer cells. The biological data show that almost all the compounds tested are active against one or more cell lines, although significant differences were observed in the antiproliferative activity: compounds **13** and

28, originated respectively by coupling of CAPE (**11**) and *n*-butyl caffeate (**19**), proved more active than 5-fluorouracil towards some cell lines and are the most lipophilic according to both experimental and calculated log *P* values. The less lipophilic amides **34–36**, though metabolically more stable than the esters, proved only moderately active. The lignan **29**, the only one that is not active toward any of the cell lines evaluated, was the least lipophilic. Microscopic observation on cell line HT116 showed that, at least for this cell line, the most active compounds **13** and **28** are effectively absorbed by the cells, presumably due to their higher lipophilicity; a significant comparison concerns the esters **28** and **32**, more lipophilic than the related amides **34** and **35**: these are less effectively absorbed and less active towards HCT-116 than the esters. It is also noteworthy that compound **27**, showing a selective activity towards SH-SY5Y cells, although less lipophilic than **13** and **28**, was more lipophilic than all the other compounds under study. The microscopic observations coupled to the lipophilicity data for the compounds under study suggest that their ability to penetrate cell membranes might be a structural feature of greater impact than the minor groove binding properties of the C1/C2 pendants.

These results, while confirming that benzoxanthene lignans are able to interact with DNA in a dual mode, reveal that their potential optimization as antitumor agents should take into account the structural features influencing their cellular uptake. In conclusion, this scarcely explored family of compounds appears worthy of further studies, also in view of their intense fluorescence, their significant antiradical properties and their possible interaction with DNA quadruplex structures, as suggested by the references cited above.

Experimental

General

All chemicals were of reagent grade and were used as purchased from Sigma-Aldrich. ESI-MS spectra were carried out in negative mode on a mass spectrometer Agilent MS G1956A using a capillary voltage of 3.5 kV. NMR spectra were run on a Varian VNMR-S spectrometer operating at 499.86 (^{1}H) and 125.70 MHz (^{13}C) and equipped with a gradient-enhanced reverse detection probe. All NMR spectrometry experiments, including two-dimensional spectra, *i.e.*, COSY, HSQC, and HMBC, were performed using software supplied by the manufacturers and acquired at a constant temperature (298 K). $CDCl_3$, CD_3OD, and $(CD_3)_2CO$ were used as solvents; chemical shifts (δ) were indirectly referred to TMS using solvent signals. STD-NMR experiments were performed on a Bruker Avance DRX 600 MHz spectrometer, equipped with a cryoprobe, at 300 K (see below for details).

LiChroprep Si-60 and LiChroprep DIOL 25–40 (Merck) were used as stationary phases for column chromatography. Thin layer chromatography (TLC) was carried out on Merck 60 F254 plates using cerium sulphate and phosphomolybdic acid as chromogenic reagents. Purity of all compounds was assessed to be greater than 95% by HPLC. Elemental analyses were performed on a Perkin-Elmer 240B microanalyzer.

The enzymatic reactions were incubated at 40 °C under shaking at 400 rpm; control reactions without enzyme were carried out under the same conditions. The progress of the chemo-enzymatic reactions was monitored at regular time intervals by TLC. Reactions were quenched on completion by filtering off the enzyme. *Candida antarctica* (Chirazyme L-2, c.-f. C2) lipase was a gift from Roche.

Preparation of esters 10, 18–20. Concd H_2SO_4 (1 mL) was added to a solution of caffeic acid (500 mg, 2.77 mmol) in MeOH, EtOH, BuOH or ethylene glycol (100 mL). The resulting mixture was stirred for 6 h at reflux. After cooling at room temperature, the solution was diluted with ethyl acetate (250 mL) and washed with an aqueous solution of $NaHCO_3$; the organic phase was washed with saturated brine, dried with anhydrous Na_2SO_4 and the solvent evaporated under vacuum to yield **10**, **18**, **19** and **20**:

*(*E*)-Methyl 3-(3,4-dihydroxyphenyl)acrylate (**10**).* Yield 99%. R_f (TLC) = 0.52 (8% MeOH–CH_2Cl_2). ^{1}H NMR data of the product are in agreement with those previously reported in the literature.[29]

*(*E*)-Ethyl 3-(3,4-dihydroxyphenyl)acrylate (**18**).* Yield 95%. R_f (TLC) = 0.66 (8% MeOH–CH_2Cl_2). ^{1}H and ^{13}C NMR data of **18** are in agreement with those previously reported in the literature.[30]

*(*E*)-Butyl 3-(3,4-dihydroxyphenyl)acrylate (**19**).* Yield 92%. R_f (TLC) = 0.60 (7% MeOH–CH_2Cl_2). ^{1}H and ^{13}C NMR data of **19** are in agreement with those previously reported in the literature.[30]

*(*E*)-2-Hydroxyethyl 3-(3,4-dihydroxyphenyl)acrylate (**20**).* Yield 90%. R_f (TLC) = 0.44 (12% EtOH–CH_2Cl_2). ^{1}H and NMR data of **20** are in perfect agreement with those previously reported in the literature.[31]

Preparation of (*E*)-2-acetoxyethyl 3-(3,4-dihydroxyphenyl)-acrylate (21). Chirazyme (218 mg) was added to a solution of **20** (220 mg, 0.98 mmol) in EtOH (50 mL) containing vinyl acetate (0.2 mL) and the suspension was kept at 40 °C under shaking (400 rpm). After 3 h incubation, the reaction was quenched by filtering off the enzyme and the filtrate was taken to dryness under reduced pressure. R_f (TLC) = 0.62 (12% EtOH–$CHCl_3$). ^{1}H NMR (500 MHz, $CDCl_3$): δ = 2.1 (s, 3H), 4.35 (m, 2H), 4.41 (m, 2H), 6.28 (d, ^3J = 16.0, 1H), 6.88 (d, ^3J = 8.5, 1H), 7.02 (dd, ^3J = 8.5, ^4J = 1.5, 1H), 7.09 (d, ^3J = 1.5, 1H), 7.60 (d, ^3J = 16.0, 1H). ^{13}C NMR (125 MHz, $CDCl_3$): δ = 20.98 (C-13), 62.26 (C-11), 62.41 (C-10), 114.40 (C-2), 114.97 (C-5), 115.49 (C-8), 122.60 (C-6), 127.37 (C-1), 143.94 (C-4), 145.82 (C-7), 146.55 (C-3), 167.38 (C-12), 171.28 (C-9).

Preparation of esters 22 and 23. A solution of caffeic acid (1.45 mmol) and tyrosol (3 mmol) or 2-(4-amminophenyl)-ethanol (3 mmol) in DMF (3 mL) was prepared and a solution of DCC and DMAP in dichloromethane (20 mL) was added; the reaction mixture was stirred mechanically at room temperature; *N*,*N*-dicyclohexylurea formed was filtered off. The organic phase was washed with a $NaHCO_3$ solution and saturated brine, dried with anhydrous Na_2SO_4 and the solvent

evaporated under vacuum. The residue was purified on a silica gel DIOL column as reported for each compound.

*(E)-4-Hydroxyphenethyl 3-(3,4-dihydroxyphenyl)acrylate (**22**).* The residue was purified on a silica gel DIOL column with 80% of $CHCl_3$–petroleum ether and subsequently with 2% of EtOH–$CHCl_3$; **22** was obtained as white powder, yield 25%. R_f (TLC) = 0.55 (10% EtOH–$CHCl_3$); ^{1}H NMR [500 MHz, $(CD_3)_2CO$]: δ = 2.06 (t, ^3J = 7.0, 2H), 2.90 (bs, 1H), 4.30 (t, ^3J = 7.0, 2H), 6.27 (d, ^3J = 16.0, 1H), 6.87 (d, ^3J = 8.0, 1H), 6.79 (d, ^3J = 8.5, 2H), 7.05 (dd, ^3J = 8.0, ^4J = 2.0, 1H), 7.13 (d, ^3J = 8.5, 2H), 7.16 (d, ^3J = 2.0, 1H), 7.54 (d, ^3J = 16.0, 1H), 8.30 (bs, 2H). ^{13}C NMR [125 MHz, $(CD_3)_2CO$]: δ = 34.1 (C-7′), 64.8 (C-8′), 114.4 (C-2), 114.8 (C-8), 115.0 (C-3′ and C-5′), 115.2 (C-5), 121.6 (C-6), 126.8 (C-1); 128.9 (C-1′), 129.9 (C-2′ and C-6′), 144.8 (C-7), 145.4 (C-3), 147.8 (C-4), 156.0 (C-4′), 166.5 (C-9).

*(E)-3-(3,4-Dihydroxyphenyl)-N-(4-hydroxyphenethyl)acrylamide (**23**).* The residue was purified on a silica gel DIOL column with a gradient of EtOH–$CHCl_3$ (from 0 to 100%); **23** was obtained as yellow powder, yield 75%. R_f (TLC) = 0.27 (12% EtOH–$CHCl_3$). ^{1}H NMR (500 MHz, CD_3OD): δ = 2.80 (t, ^3J = 7.0, 2H), 3.74 (t, ^3J = 7.0, 2H), 7.06 (d, ^3J = 2.0, 1H), 6.55 (d, ^3J = 16.0, 1H), 6.79 (d, ^3J = 8.0, 1H), 6.95 (dd, ^3J = 8.0, ^4J = 2.0, 1H), 7.20 (d, ^3J = 8.5, 2H), 7.53 (d, ^3J = 16.0, 1H), 7.57 (d, ^3J = 8.5, 2H). ^{13}C NMR (125 MHz, CD_3OD): δ = 38.3 (C-7′), 62.8 (C-8′), 113.8 (C-2), 115.1 (C-5), 117.4 (C-8), 119.9 (C-3′ and C-5′), 120.9 (C-6), 126.9 (C-1), 128.9 (C-2′ and C-6′), 134.9 (C-1′), 136.9 (C-4′), 141.8 (C-7), 145.4 (C-3), 147.6 (C-4), 166.0 (C-9).

Preparation of amides 24–26. The caffeic acid (300 mg, 1.62 mmol) is dissolved in 8 mL of DMF and 0.23 mL of triethylamine (1.62 mmol). The solution is cooled in an ice-water bath and 1.62 mmol of the amine are added followed by a solution of BOP (733 mg, 1.62 mmol) in 10 mL of CH_2Cl_2. The mixture is stirred at 0 °C for 30 min and then at room temperature for 24 h. CH_2Cl_2 is removed under reduced pressure and the solution is diluted with 40 mL of water. The mixture is extracted with ethyl acetate. The extract is washed successively with 1 M HCl, 1 M $NaHCO_3$, and water, dried over Na_2SO_4, filtered and evaporated. The residue is purified on a silica gel DIOL column as reported for each compound.

*(E)-N-Butyl-3-(3,4-dihydroxyphenyl)acrylamide (**24**).* The residue was purified on a silica gel DIOL column with an eluent 60% ethyl acetate–petroleum ether; **24** was obtained as white powder, yield 58%. R_f (TLC) = 0.50 (8% MeOH–CH_2Cl_2). ^{1}H NMR (CD_3OD, 500 MHz): δ = 0.94 (t, ^3J = 7.5, 3H), 1.38 (m, 2H), 1.53 (m, 2H), 3.28 (t, ^3J = 7.0, 2H), 4.89 (s, OH and NH), 6.38 (d, ^3J = 15.3, 1H, H-7), 6.76 (d, ^3J = 8.5, 1H, H-5), 6.96 (dd, ^3J = 8.0, ^4J = 1.5, 1H, H-6), 7.01 (d, ^3J = 2.0, 1H, H-2), 7.40 (d, ^3J = 15.3, 1H, H-8). ^{1}H NMR data of **24** are in agreement with those previously reported in the literature.[32] ^{13}C NMR (CD_3OD, 125 MHz) δ = 12.7 (C-14), 19.8 (C-13), 31.2 (C-12), 38.9 (C-11), 113.7 (C-2), 115.1 (C-5), 117.1 (C-8), 120.7 (C-6), 127.0 (C-1), 140.7 (C-7), 145.3 (C-4), 147.3 (C-3), 169.8 (C-9).

*(E)-3-(3,4-Dihydroxyphenyl)-N-(4-hydroxyphenethyl)acrylamide (**25**).* The residue was purified on a silica gel DIOL column with a gradient of MeOH–CH_2Cl_2 (from 0 to 10%); **25** was obtained as white powder, yield 74%. R_f (TLC) = 0.76 (10% EtOH–EtOAc). ^{1}H and ^{13}C NMR data of **23** are in perfect agreement with those previously reported in the literature.[33]

*(E)-3-(3,4-Dihydroxyphenyl)-N,N-diethylacrylamide (**26**).* The residue was purified on a silica gel DIOL column with a gradient of EtOAc–petroleum ether (from 30 to 50%); **26** was obtained as white powder, yield 50%. R_f (TLC) = 0.41 (10% EtOAc–petroleum ether). ^{1}H NMR (CD_3OD, 500 MHz): δ = 1.17 (t, ^3J = 7.0, 3H), 1.25 (t, ^3J = 7.0, 3H), 3.46 (m, 2H), 3.52 (m, 2H), 4.88 (s, OH), 6.76 (d, ^3J = 15.3, 1H, H-7), 6.78 (d, ^3J = 8.5, 1H, H-5), 6.96 (dd, ^3J = 8.5, ^4J = 2.0, 1H, H-6), 7.05 (d, ^3J = 2.0, 1H, H-2), 7.47 (d, ^3J = 15.3, 1H, H-8). ^{1}H NMR data of **26** are in agreement with those previously reported in the literature.[34] ^{13}C NMR (CD_3OD, 125 MHz): δ = 12.1 (C-13), 13.8 (C-11), 41.0 (C-12), 42.2 (C-10), 113.7 (C-2), 113.9 (C-8), 115.1 (C-5), 120.8 (C-6), 127.2 (C-1), 143.0 (C-7), 145.3 (C-4), 147.5 (C-3), 167.2 (C-9).

Synthesis of compounds 12 and 13. Dimethyl 6,9,10-trihydroxybenzo[*k*,*l*]xanthene-1,2-dicarboxylate (**12**) and bis(2-phenylethyl)-6,9,10-trihydroxybenzo[*k*,*l*]xanthene-1,2-dicarboxylate (**13**) were synthesized as previously described.[7]

Synthesis of compounds 27–36. To a solution of caffeic ester or caffeic amides (0.70 mmol) dissolved in $CHCl_3$ (50 mL), $CHCl_3$–EtOH (9–1) or in EtOH was added $Mn(OAc)_3$ (substrate : oxidative agent ratio 1 : 4). The reaction mixtures were stirred for 3–8 h at room temperature; the progress of the reactions was monitored at regular time intervals by TLC; the solvent was evaporated *in vacuo* and the residue was treated with a saturated solution of ascorbic acid in H_2O; subsequently the mixture was extracted twice with EtOAc; the organic phase, after washing with a solution of $NaHCO_3$ and saturated brine, was dried over anhydrous Na_2SO_4 and the solvent evaporated under *vacuum*. The residue was purified on a chromatographic column as reported for each compound. In the following, the assignments of NMR signals for the side chains are referred to the numbering system reported in ESI.†

*Diethyl 6,9,10-trihydroxybenzo[*k,l*]xanthene-1,2-dicarboxylate (**27**).* The residue was purified on a silica gel DIOL column with a gradient of CH_2Cl_2–MeOH (from 0 to 2%); **27** was obtained as yellow powder, yield 47%. R_f (TLC) = 0.55 (6% MeOH–CH_2Cl_2). ^{1}H NMR [500 MHz, $(CD_3)_2CO$]: δ = 1.382 (t, ^3J = 7.0, 3H, H-2‴), 1.387 (t, ^3J = 7.0, 3H, H-2″), 4.35 (m, ^3J = 7.0, 2H, H-1‴), 4.37 (m, ^3J = 7.0, 2H, H-1″), 6.72 (s, 1H, H-8), 7.26 (s, 1H, H-11), 7.34 (d, ^3J = 8.5, 1H, H-5), 7.52 (d, ^3J = 8.5, 1H, H-4), 8.15 (s, 1H, H-3) ppm. ^{13}C NMR [125 MHz, $(CD_3)_2CO$]: δ = 13.2 (C-2″), 13.6 (C-2‴), 60.9 (C-1″), 61.2 (C-1‴), 103.8 (C-8), 110.0 (C-11a), 111.5 (C-11), 119.6 (C-5), 121.1 (C-4), 121.2 (C-1), 123.3 (C-11c), 124.1 (C-2), 125.5 (C-11b), 126.7 (C-3a), 128.5 (C-3), 141.7 (C-10), 141.9 (C-6), 146.9 (C-9), 148.2 (C-7a), 165.9 (CO-2′), 169.9 (CO-1′) ppm. ESI-MS *m*/*z* 408.8 $[M - H]^-$; elemental analysis C, 64.39 and H, 4.42 calculated for $C_{22}H_{18}O_8$. Found C, 64.72 and H, 4.38.

*Dibutyl 6,9,10-trihydroxybenzo[*k,l*]xanthene-1,2-dicarboxylate (**28**).* The residue was purified on a silica gel DIOL column with a gradient of MeOH–CH_2Cl_2 (from 0 to 3%); **28** was obtained as yellow powder, yield 40%. R_f (TLC) = 0.5 (8% MeOH–CH_2Cl_2). ^{1}H NMR [500 MHz, $(CD_3)_2CO$]: δ = 0.94 (t, ^3J =

7.0, 3H, H-4″), 0.99 (t, ^3J = 7, 3H, H-4‴), 1.44 (m, ^3J = 7.5, 2H, H-3″), 1.49 (m, ^3J = 7.5, 2H, H-3‴), 1.74 (m, ^3J = 7.5, 4H, H-2″ and H-2‴), 4.40 (t, ^3J = 6.5, 2H, H-1‴), 4.30 (t, ^3J = 6.5, 2H, H-1″), 6.71 (s, 1H, H-8), 7.25 (s, 1H, H-11), 7.31 (d, ^3J = 9.0, 1H, H-5), 7.45 (d, ^3J = 9.0, 1H, H-4), 8.16 (s, 1H, H-3) ppm. ^{13}C NMR [125 MHz, $(CD_3)_2CO$]: δ = 13.1 (C-4″), 13.1 (C-4‴), 19.0 (C-3″ and C-3‴), 30.1 (C-2″), 30.6 (C-2‴), 64.7 (C-1″), 65.2 (C-1‴), 103.8 (C-8), 110.1 (C-11a), 111.5 (C-11), 119.7 (C-5), 121.2 (C-4), 121.3 (C-1), 123.3 (C-11c), 124.1 (C-2), 125.5 (C-11b), 126.7 (C-3a), 128.5 (C-3), 136.7 (C-6a), 141.71 (C-10), 141.78 (C-6), 146.9 (C-9), 148.1 (C-7a), 165.9 (CO-2′), 170.0 (CO-1′) ppm. ESI-MS *m*/*z* 464.9 $[M - H]^-$, elemental analysis C, 66.94 and H, 5.62 calculated for $C_{26}H_{26}O_8$. Found C, 66.85 and H, 5.60.

*Bis(2-hydroxyethyl)-6,9,10-trihydroxybenzo[*k,l*]xanthene-1,2-dicarboxylate (**29**).* The residue was purified on a silica gel DIOL column with a gradient of EtOH–$CHCl_3$ (from 3 to 5%); for direct dimerization of **20**, **29** was obtained as yellow powder, yield 12.8%; R_f (TLC) = 0.32 (8% EtOH–$CHCl_3$); ^{1}H NMR [500 MHz, $(CD_3)_2CO$] of **29**: δ = 3.88 (*b*t, 2H, H-2‴), 3.97 (*b*t, 2H, H-2″), 4.36 (*b*t, 2H, H-1‴), 4.54 (*b*t, 4H, H-1″), 6.69 (s, 1H, H-8), 7.33 (d, ^3J = 8.5, 1H, H-5), 7.42 (s, 1H, H-11), 7.52 (d, ^3J = 8.5, 1H, H-4), 8.25 (s, 1H, H-3). ^{13}C NMR [125 MHz, $(CD_3)_2CO$]: δ = 59.9 (C-2‴), 60.1 (C-2″), 67.0 (C-1‴), 67.3 (C-1″), 104.6 (C-8), 110.8 (C-11a), 112.3 (C-11), 120.5 (C-5), 121.9 (C-1), 122.0 (C-4), 124.1 (C-11c), 124.7 (C-11b), 125.8 (C-2), 127.4 (C-3a), 129.7 (C-3), 137.4 (C-6a); 142.4 (C-10), 142.7 (C-6), 147.6 (C-9), 148.9 (C-7a), 166.8 (C-2′), 170.9 (C-1′). ESI-MS *m*/*z* 440.8 $[M - H]^-$, elemental analysis C, 59.73 and H, 4.10 calculated for $C_{22}H_{18}O_8$. Found C, 59.79 and H, 4.12.

*Bis(2-acetoxyethyl)6,9,10-trihydroxybenzo[*k,l*]xanthene-1,2-dicarboxylate (**30**).* The residue was purified on a silica gel DIOL column with a gradient of EtOH–CH_2Cl_2 (from 0 to 3%); **30** was obtained as yellow-green powder, yield 45%. R_f (TLC) = 0.55 (10% EtOH–$CHCl_3$). ^{1}H NMR [500 MHz, $(CD_3)_2CO$]: δ = 1.98 (s, 3H, H-4″), 2.07 (s, 3H, H-4‴), 4.43 (bt, 4H, H-2″ and H-2‴), 4.54 (bt, 2H, H-1″), 4.64 (bt, 2H, H-1‴), 6.73 (s, 1H, H-8), 7.25 (s, 1H, H-11), 7.35 (d, ^3J = 8.5, 1H, H-5), 7.53 (d, ^3J = 8.5, 1H, H-4), 8.21 (s, 1H, H-3). ^{13}C NMR [125 MHz, $(CD_3)_2CO$]: δ = 20.4 (C-4″), 20.5 (C-4‴), 62.2 (C-2″), 62.5 (C-2‴), 63.8 (C-1″), 64.3 (C-1‴), 104.5 (C-8), 110.6 (C-11a), 112.0 (C-11), 120.5 (C-5), 121.2 (C-1), 122.1 (C-4), 124.0 (C-11c), 125.0 (C-11b), 125.4 (C-2), 127.4 (C-3a), 129.7 (C-3), 137.4 (C-6a), 142.4 (C-10), 142.7 (C-6), 147.6 (C-9), 148.9 (C-7a), 166.3 (C-2′), 170.4 (C-1′), 170.8 (C-3″ and C-3‴). ESI-MS *m*/*z* 524.8 $[M - H]^-$, elemental analysis C, 59.32 and H, 4.21 calculated for $C_{26}H_{22}O_{12}$. Found C, 59.41 and H, 4.17.

*2-(2-Acetoxyethyl)1-(2-hydroxyethyl)6,9,10-trihydroxybenzo[*k,l*]-xanthene-1,2-dicarboxylate (**31**).* The substrate **30** (22 mg, 0.04 mmol) was dissolved in EtOAc (12 mL) and *n*-BuOH (1 mL). *Candida antarctica* lipase (24 mg) was added to this solution and the mixture was maintained under shaking at 40 °C for 72 h. The reaction was quenched by filtering off the enzyme and the filtrate was evaporated *in vacuo*. The residue was purified on a silica gel DIOL column with a gradient of EtOH–$CHCl_3$ (from 0 to 3%) to obtain the deacylated analogues **31** (8.5 mg, 70% yield) and **29** (3.6 mg, 30% yield) and the unconverted substrate (9.9 mg, 45%). ^{1}H NMR [500 MHz, $(CD_3)_2CO$] of **31**: δ = 1.98 (s, 3H, H-4‴), 3.90 (*b*t, 2H, H-2″), 4.39 (*b*t, 2H, H-1″), 4.43 (*b*t, 2H, H-2‴), 4.64 (*b*t, 2H, H-1‴), 6.73 (s, 1H, H-8), 7.25 (s, 1H, H-11), 7.34 (d, ^3J = 8.5, 1H, H-5), 7.52 (d, ^3J = 8.5, 1H, H-4), 8.25 (s, 1H, H-3). ^{13}C NMR [125 MHz, $(CD_3)_2CO$]: δ = 20.4 (C-4‴), 60.6 (C-2″), 62.6 (C-2‴), 64.3 (C-1‴), 67.7 (C-1″), 104.6 (C-8), 110.7 (C-11a), 112.3 (C-11), 120.5 (C-5), 121.9 (C-4), 122.1 (C-1), 124.0 (C-11c), 125.0 (C-11b), 125.8 (C-2), 127.5 (C-3a), 142.5 (C-10), 147.6 (C-9), 149.0 (C-7a), 166.6 (C-2′), 170.7 (C-1′), 170.8 (C-3‴). Selected HMBC correlations: C (H), 166.6 (8.25; 4.39), 170.8 (4.43; 1.98), 170.7 (4.64), 60.6 (4.39). ESI-MS *m*/*z* 482.8 $[M - H]^-$, elemental analysis C, 59.11 and H, 4.16 calculated for $C_{24}H_{20}O_{11}$. Found C, 59.48 and H, 4.17.

*Bis(4-hydroxyphenethyl)6,9,10-trihydroxybenzo[*k,l*]xanthene-1,2-dicarboxylate (**32**).* The residue was purified on a silica gel DIOL column with a gradient of EtOH–CH_2Cl_2 (from 0 to 7%); **32** was obtained as yellow powder, yield 55%. R_f (TLC) = 0.47 (12% EtOH–$CHCl_3$).

^{1}H NMR (500 MHz, CD_3OD): δ = 2.93 (t, ^3J = 8.0, 2H, H-2‴), 2.97 (t, ^3J = 7.0 2H, H-2″), 4.43 (t, ^3J = 7.0, 2H, H-1″), 4.56 (t, ^3J = 8.0, 2H, H-1‴), 6.69 (d, ^3J = 8.5, 2H, H-3^{IV} and H-5^{IV}), 6.71 (s, 1H, H-8), 6.75 (d, ^3J = 8.0, 2H, H-3^{V} and H-5^{V}), 7.10 (m, 5H, H-11, H-2^{IV}, H-6^{IV}, H-2^{V} and H-6^{V}), 7.21 (d, ^3J = 8.5, 1H, H-5), 7.32 (d, ^3J = 8.5, 1H, H-4), 7.94 (s, 1H, H-3). ^{13}C NMR (125 MHz, CD_3OD): δ = 33.3 (C-2‴), 33.8 (C-2″), 66.0 (C-1″), 66.8 (C-1‴), 103.5 (C-8), 109.6 (C-11a), 111.2 (C-11), 114.9 (C-3^{IV} and C-5^{IV}), 115.0 (C-3^{V} and C-5^{V}), 118.5 (C-1), 119.4 (C-5), 120.2 (C-2), 120.9 (C-4), 123.3 (C-11c), 124.5 (C-1^{IV}), 124.7 (C-11b and C-1^{V}), 126.6 (C-3a), 128.6 (C-3), 129.6 (C-2^{IV} and C-6^{IV}), 129.7 (C-2^{V} and C-6^{V}), 136.9 (C-6a), 141.7 (C-6), 141.8 (C-7a), 147.0 (C-10), 148.3 (C-9), 155.5 (C-4^{IV}), 155.7 (C-4^{V}), 166.4 (C-2′), 171.6 (C-1′). ESI-MS: *m*/*z* 592.8 $[M - H]^-$, elemental analysis C, 68.68 and H, 4.41 calculated for $C_{34}H_{26}O_{10}$. Found C, 68.61 and H, 4.39.

*Bis(4-aminophenethyl)6,9,10-trihydroxybenzo[*k,l*]xanthene-1,2-dicarboxylate (**33**).* The residue was purified on a silica gel DIOL column with a gradient of EtOH–$CHCl_3$ (from 5 to 13%); **33** was obtained as yellow powder, yield 25%. R_f (TLC) = 0.44 (20% EtOH–CH_2Cl_2). ^{1}H NMR (500 MHz, CD_3OD): δ = 2.79 (m, 4H, H-2″ and H-2‴), 3.74 (t, ^3J = 7.0, 4H, H-1″ and H-1‴), 6.61 (s, 1H, H-8), 7.13 (m, 6H, H-4, H-5, H-2^{IV}, H-6^{IV}, H-2^{V} and H-6^{V}), 7.30 (s, 1H, H-11), 7.56 (m, 5H, H-3, H-3^{IV}, H-5^{IV}, H-3^{V} and H-5^{V}). ^{13}C NMR (125 MHz, CD_3OD): δ = 39.70 (C-2‴)*^{1}, 39.73 (C-2″)*^{1}, 64.2 (C-1″ and C-1‴), 104.7 (C-8), 111.6 (C-11a), 113.8 (C-11), 119.9 (C-11b), 120.2 (C-5), 121.3 (C-4), 122.0 (C-3^{IV} and C-5^{IV})*^{4}, 122.6 (C-3^{V} and C-5^{V})*^{4}, 123.8 (C-1), 124.1 (C-11c), 125.8 (C-3), 128.2 (C-3a), 130.0 (C-2^{V} and C-6^{V})*^{3}, 130.1 (C-2^{IV} and C-6^{IV})*^{3}, 133.4 (C-2), 136.3 (C-1^{IV})*^{2}, 136.7 (C-1^{V})*^{2}, 137.8 (C-6a), 138.1 (C-4^{IV})*^{5}, 138.2 (C-4^{V})*^{5}, 141.7 (C-6), 142.9 (C-7a), 148.4 (C-10), 149.4 (C-9), 169.7 (C-2′), 171.3 (C-1′). *^{n}: *interchangeable with n*. ESI-MS: *m*/*z* 590.7 $[M - H]^-$, elemental analysis C, 68.91, H, 4.76, and N, 4.73 calculated for $C_{34}H_{28}N_2O_8$. Found C, 68.87, H, 4.72 and N, 4.75.

N,N-*Dibutyl-6,9,10-trihydroxybenzo[*k,l*]xanthene-1,2-dicarboxamide (**34**).* The residue was purified on a silica gel DIOL

column with a gradient of MeOH–CH_2Cl_2 (from 0 to 3%); **34** was obtained as yellow-green powder, yield 15%. R_f (TLC) = 0.53 (8% MeOH–CH_2Cl_2). ^{1}H NMR [500 MHz, $(CD_3)_2CO$]: δ = 0.94 (m, 6H, H-4″ and H-4‴), 1.46 (m, 4H, H-3″ and H-3‴), 1.62 (m, 4H, H-2″ and H-2‴), 3.43 (q, ^3J = 6.0, 2H, H-1″), 3.74 (m, 2H, H-1‴), 6.62 (s, 1H, H-8), 7.20 (d, ^3J = 8.0, 1H, H-5), 7.30 (d, ^3J = 8.0, 1H, H-4), 7.38 (t, ^3J = 6.0, 1H, NH), 7.51 (s, 1H, H-11), 7.61 (s, 1H, H-3), 7.65 (t, 6.0, ^3J = 1H, NH). ^{13}C NMR [125 MHz, $(CD_3)_2CO$]: δ = 14.1 (C-4″ and C-4‴), 20.7 (C-3‴), 20.9 (C-3″), 31.5 (C-2‴), 32.4 (C-2″), 40.1 (C-1‴), 40.5 (C-1″), 104.3 (C-8), 111.8 (C-11a), 113.2 (C-11), 119.0 (C-5), 120.7 (C-4), 123.2 (C-11c), 124.1 (C-11b), 124.7 (C-1), 125.6 (C-3), 127.0 (C-3a), 133.0 (C-2), 137.5 (C-6a), 140.0 (C-6), 142.3 (C-7a), 147.5 (C-10), 148.5 (C-9), 168.7 (C-2′), 171.4 (C-1′). ESI-MS: m/z 463.3 $[M - H]^-$, elemental analysis C, 67.23, H, 6.08 and N, 6.03 calculated for $C_{26}H_{28}N_2O_6$. Found C, 67.12, H, 6.02 and N, 6.09.

6,9,10-Trihydroxy-N,N-*bis(4-hydroxyphenethyl)benzo[*k,l*]-xanthene-1,2-dicarboxamide (**35**).* The residue was purified on a silica gel DIOL column with a gradient of MeOH–CH_2Cl_2 (from 0 to 4%); **35** was obtained as yellow-green powder, yield 20%. R_f (TLC) = 0.21 (17% MeOH–$CHCl_3$). ^{1}H NMR (500 MHz, CD_3OD): δ = 2.82 (t, ^3J = 7.5, 4H, H-2″ and H-2‴), 3.55 (t, ^3J = 7.5, 4H, H-1″ and H-1‴), 6.69 (s, 1H, H-8), 6.70 (d, ^3J = 8.5, 2H, H-3^{IV} and H-5^{IV}), 6.75 (d, ^3J = 8.5, 2H, H-3^{V} and H-5^{V}), 7.13 (d, ^3J = 8.5, 2H, H-2^{V} and H-6^{V}), 7.19 (d, ^3J = 8.5, 1H, H-5), 7.26 (d, ^3J = 8.5, 1H, H-4), 7.36 (s, 1H, H-11), 7.42 (s, 1H, H-3). ^{13}C NMR (125 MHz, CD_3OD): δ = 33.2 (C-2‴), 33.5 (C-2″), 41.4 (C-1″), 41.8 (C-1‴), 103.3 (C-8), 110.2 (C-11), 112.2 (C-11a), 114.9 (C-3^{IV}, C-5^{IV}, C-3^{V} and C-5^{V}), 119.0 (C-11c), 119.7 (C-5), 124.2 (C-3), 124.3 (C-4), 122.6 (C-1), 127.0 (C-3a), 129.3 (C-2^{IV}, C-6^{IV}, C-2^{V} and C-6^{V}), 129.5 (C-1^{IV} and C-1^{V}), 129.9 (C-2), 131.9 (C-11b), 136.9 (C-6a), 140.3 (C-10), 141.6 (C-6), 147.0 (C-9), 148.0 (C-7a), 155.4 (C-4^{IV}), 155.5 (C-4^{V}), 170.2 (C-1′), 171.4 (C-2′). ESI-MS: m/z 591.3 $[M - H]^-$, elemental analysis C, 68.91, H, 4.76, and N, 4.73 calculated for $C_{34}H_{28}N_2O_8$. Found C, 68.75, H, 4.72 and N, 4.78.

N,N,N,N-*Tetraethyl-6,9,10-trihydroxybenzo[*k,l*]xanthene-1,2-dicarboxamide (**36**).* The residue was purified on a silica gel DIOL column with a gradient of MeOH–CH_2Cl_2 (from 0 to 2%); **36** was obtained as yellow-brown powder, yield 35%. R_f (TLC) = 0.44 (50% EtOAc–petroleum ether). ^{1}H NMR [500 MHz, $(CD_3)_2CO$]: δ = 0.92 (t, ^3J = 7.0, 3H, H-4‴), 1.13 (t, ^3J = 7.0, 3H, H-2″), 1.19 (t, ^3J = 7.0, 3H, H-4″), 1.23 (t, ^3J = 7.0, 3H, H-2‴), 3.01 (bs, 1H, -OH), 3.19 (m, 2H, H-3‴), 3.40 (m, 2H, H-1″), 3.58 (m, 2H, H-3″), 3.74 (m, 2H, H-1‴), 6.67 (s, 1H, H-8), 7.24 (d, ^3J = 9.0, 1H, H-5), 7.34 (d, ^3J = 9.0, 1H, H-4), 7.37 (s, 1H, H-3), 7.44 (s, 1H, H-11), 8.41 (bs, 2H, -OH). ^{13}C NMR [125 MHz, $(CD_3)_2CO$]: δ = 12.1 (C-2‴), 12.8 (C-4″), 13.2 (C-4‴), 13.9 (C-2″), 39.2 (C-1″), 39.3 (C-1‴), 43.0 (C-3″), 43.8 (C-3‴), 104.2 (C-8), 111.6 (C-11a), 113.0 (C-11), 119.8 (C-5), 120.3 (C-4), 122.2 (C-11c), 122.4 (C-3), 123.1 (C-2 and C-11b), 127.9 (C-3a), 133.7 (C-1), 137.4 (C-6a), 142.3 (C-7a), 140.6 (C-6), 147.3 (C-10), 148.4 (C-9), 169.8 (C-2′), 170.2 (C-1′). ESI-MS: m/z 463.3 $[M - H]^-$, elemental analysis C, 67.23, N, 6.08 and H, 6.03 calculated for $C_{26}H_{28}N_2O_6$, found C, 66.98, H, 6.05 and N, 6.00.

Measurements of the capacity factor (*K*)

The measurements of the capacity factor were performed using a Luna-C18 column (5 μm; 4.6 × 250 mm; Phenomenex) using as an eluent a gradient of H_2O–CH_3CN; the elution gradient had the following profile: $t_{0\ min}$ B (5%), $t_{10\ min}$ B (100%), $t_{15\ min}$ B (100%). The flow rate was 1 mL min^{-1}. All experiments were performed using an Agilent 1100 pump, a photodiode array detector Agilent Series 1200 G1315C/D; an autosampler Series 1100 G1313A (Agilent) was used for sample injections. The capacity factor K was calculated using the following expression:

$$K = (t_R - t_o)/t_o$$

where t_R is the retention time of the tested substance, and t_o is the dead-time determined using ascorbic acid as an analyte.

Calculated log P values were obtained with ACD/labs log P program version 11.

DF-STD NMR

As the compounds under study were not water soluble, preliminary solubility tests were carried out on compounds **27–36** before the NMR measurements; as a result, different DMSO–water mixtures containing buffered solution (10 mM of NaCl, 10 mM of NaH_2PO_4) at pH 7.4 were used to solve the molecules. For **27** and **30–36** the final concentration was 1 mM and for the DNA, 50 μM (expressed as molarity of phosphate groups), in 200 μl of the following solvent: $[D_6]$DMSO–D_2O 50/150 for **32**, **33** and **35** and 10/190 for **27**, **30**, **31**, **34** and **36**. The final concentration of **28** and **29** was 0.5 mM *vs.* 25 μM of DNA, by using the solvent mixture $[D_6]$DMSO–D_2O in the ratio 10/190; for **12** and **13** see literature data.[15]

The DNA used as a biological target was a poly(dG–dC)·poly(dG–dC) copolymer, presenting an average of 750 base pairs. The copolymer was dissolved in the above described buffer aqueous solution and underwent annealing for 5 min at 80 °C. The copolymer was dried and then dissolved in the deuterated buffer with the percentage of DMSO as described above.

Two STD NMR spectra for each ligand were recorded irradiating on the aromatic and sugar proton resonances (Table 3) of DNA by Gaussian train pulses reaching a total saturation time of 4 s.

For each DF-STD spectrum (saturation time = 4 s) 288 scans were recorded, whereas 144 scans were recorded for the reference STD spectrum. The water ^{1}H signal was suppressed using a 3–9–19[35] pulse sequence. The STD effects of the individual protons were calculated for each compound relative to a reference spectrum with off-resonance saturation at δ = −16 ppm.

In our original contribution, based on the analysis of ligands with a well-known binding mode to DNA, we defined three BMI ranges: 0 < BMI < 0.50 for external (nonspecific), electrostatic backbone binding; 0.90 < BMI < 1.10 for minor groove binding; and 1.20 (0.90) < BMI < 1.50 for base-pair intercalation.[21]

Table 3 Irradiation resonances used in the STD NMR experiments for **12**, **13** and **27–36**

	Saturation frequency (ppm)	
Compound	Aromatic	Aliphatic
12[a]	9.0	2.0
13[a]	9.2	1.3
27	8.8	5.4
28	9.2	5.4
29	9.0	2.5
30	9.0	3.2
31	8.7	5.8
32	8.8	5.4
33	8.5	5.0
34	9.0	5.1
35	8.5	5.0
36	8.8	5.4

[a] Values for **12** and **13** are reported from our previous work.[15]

The BMI were calculated using the following equation:[21]

$$\mathrm{BMI} = \frac{\sum_i \left(\frac{\mathrm{SN}_{\mathrm{aromatic}}/\mathrm{SN}_{\mathrm{rif}}}{\mathrm{SN}_{\mathrm{aliphatic}}/\mathrm{SN}_{\mathrm{rif}}}\right)}{n_i} \quad (1)$$

where $\mathrm{SN}_{\mathrm{aromatic}}$ and $\mathrm{SN}_{\mathrm{aliphatic}}$ are the signal to noise ratios of the ligand peaks obtained from the on-resonance STD spectra irradiating in the aromatic and aliphatic regions, respectively. $\mathrm{SN}_{\mathrm{rif}}$ is instead the intensity of the same signal in the off-resonance spectrum (saturation at $\delta = -16$ ppm), and n_i is the number of ligand signals.

Computational methods

As described in our previous paper,[15] Models A and B were built using the graphical interface Maestro version 6.0, Schrödinger, LLC, New York, NY, 2003. A B-DNA decamer (dG–dC)·(dG–dC) was built, in order to have a complete helix turn, using the available base pair models of Maestro (see ESI† for the three-dimensional coordinates of the models). To study the intercalation between base pairs, the binding site was built taking into account the distances from experimental structures of complexes between nucleic acids and intercalators and the induced local unwinding. Two intercalation points were built (Models A and B), and considered in the calculations. In detail, the binding site of Model A was formed by the G3·C13 and C4·G14 base pairs, whereas for Model B the intercalation point was delimited by C4·G14 and G5·C15 base pairs. Both models were optimized using Macromodel 8.5 software[36] by the Polak–Ribiere Conjugate Gradient method using the Force Field Amber[37] (threshold 0.005 kJ mol^{-1} $\mathrm{Å}^{-1}$). The GB/SA (Generalized Born/surface area)[38] solvent treatment was used, mimicking the presence of H_2O, in the calculations for reducing the artifacts derived from the absence of the solvent. During the optimization of the geometries and energies of Models A and B, a penalty of 100 kJ $\mathrm{Å}^{-2}$ was applied for the distance violations along the hydrogen bonds between nucleotide aromatic rings of each complementary strand.

All ligand structures were built and their geometries optimized through the MacroModel 8.5 software[36] package and using the MMFFs force field.[39] The MonteCarlo Multiple Minimum (MCMM) method (10 000 steps) of the MacroModel package[36] was used in order to allow a full exploration of the conformational space. The so-obtained geometries were optimised using the Polak–Ribier Conjugate Gradient algorithm (PRCG, maximum derivative less than 0.001 kcal mol^{-1}).

Autodock 4.2[40] was used for all docking calculations. The software rapidly takes into account the ligand–macromolecule interactions by precalculating atomic affinity potentials (*grid maps*) for each atom type in the substrate molecule by the grid method. These maps are calculated by AutoGrid, where the protein is embedded in a three-dimensional grid and a probe atom is placed at each grid point. The energy of interaction of this single atom with the protein is assigned to the grid point.

For all the docking calculations with Models A and B, a grid box size of 54 × 54 × 52 with a spacing of 0.375 Å between the grid points was used and centred on the following x, y and z coordinates: −1.189; 2.505; 23.5 (Model A), and −1.189; 2.505; 20.2 (Model B). The above described grid boxes included the external deoxyribose/backbone.

In order to achieve a representative conformational space during the docking calculations on ligands under investigation, ten calculations consisting of 256 runs were performed, obtaining 2560 ligand conformations (256 × 10). The Lamarckian genetic algorithm was used for dockings. An initial population of 700 randomly placed individuals, a maximum number of 6×10^6 energy evaluations, and a maximum number of 7×10^6 generations were taken into account. A mutation rate of 0.02, a crossover rate of 0.8 and a local search frequency of 0.26 were used. All the 3D models were depicted using the Phyton software.

Human cell cultures

The lung carcinoma cell line A549 (ATCC number: CCL-185), the lung squamous carcinoma cell line NCI-H226 (ATCC number: CRL-5826), the colorectal adenocarcinoma Caco-2 (ATCC number: HTB-37) and the HT29 (ATCC number: HTB-38) were obtained from the American Type Culture Collection (ATCC, Teddington, UK). The SH-SY5Y (ATCC CRL-2266) was kindly provided by Prof. Maria Angela Sortino (University of Catania, Italy). The A549, NCI-H226 and Caco-2 cell lines were grown in RPMI 1640 medium (cat. 61870-010, GIBCO by Life Technologies, Italy). The HT-29 cells were grown in DMEM with glutamax (4.5 g L^{-1}) (cat. no. 31965-023, GIBCO by Life Technologies, Italy). The SH-SY5Y cells were grown in DMEM-F12 (cat. no. 21331-046, GIBCO by Life Technologies, Italy). All media were supplemented with 10% (vol/vol) heat-inactivated foetal bovine serum, 2 mM L-alanyl-L-glutamine, penicillin-streptomycin (50 units – 50 mg per ml) and cell cultures were incubated at 37 °C under a humidified atmosphere of 5% CO_2, 95% air. The culture media were changed twice a week.

Treatment with antitumor compounds and MTT colorimetric assay

Human cancer cell lines (2.5–3 × 10^3 cells per 0.33 cm^2) were plated in 96 well plates "Nunclon TM Microwell TM" (Nunc), and were incubated at 37 °C. Treatment with antitumor molecules, cytotoxicity and cell proliferation was conducted as previously described. After 24 h, cells were treated with the compounds (final concentration 0.01–100 μM). Cells treated with 0.5–1% of DMSO were used as controls. Microplates were incubated at 37 °C under a humidified atmosphere of 5% CO_2, 95% air for 3 days and then cytotoxicity was measured with the colorimetric assay based on the use of tetrazolium salt MTT (3 (4,5 dimethylthiazol-2-yl)-2,5-diphenyl tetrazolium bromide). The results were read on a multiwell scanning spectrophotometer (Multiscan reader) using a wavelength of 570 nm. Each value was the average of 8 wells (standard deviations were less than 10%). The GI_{50} value was calculated according to NCI: thus, GI_{50} is the concentration of the test compound where $100 \times (T - T_0)/(C - T_0) = 50$ (where T is the optical density of the test well after a 72 h period of exposure to the test compound, T_0 is the optical density at time zero, and C is the DMSO control optical density). The cytotoxicity effect was calculated according to NCI when the optical density of treated cells was lower than the T_0 value using the following formula: $100 \times (T - T_0)/T_0 < 0$.

Acknowledgements

This research was supported by MIUR, Ministero dell'Università e della Ricerca (PRIN 2009, Rome, Italy), and by grants from the Università degli Studi di Catania (Progetti di Ricerca di Ateneo, Catania, Italy) and Università di Salerno.

Notes and references

1 (*a*) J. Clardy and C. Walsh, *Nature*, 2004, **432**, 829–837; (*b*) A. D. Kinghorn, L. Pan, J. N. Fletcher and H. Y. Chai, *J. Nat. Prod.*, 2011, **74**, 1539–1555; (*c*) C. Spatafora and C. Tringali, Natural Polyphenols to Synthetic Antitumor Agents, in: *Bioactive Compounds from Natural Sources, Natural Products as Lead Compounds in Drug Discovery*, II edn, CRC Press-Taylor & Francis, 2012, pp. 299–338; (*d*) D. J. Newman and G. M. Cragg, *J. Nat. Prod.*, 2012, **75**, 311–335.

2 T. A. Johnson, J. Sohn, W. D. Inman, S. A. Estee, S. T. Loveridge, H. C. Vervoort, K. Tenney, J. K. Liu, K. K. H. Ang, J. Ratnam, W. M. Bray, N. C. Gassner, Y. Y. Shen, R. S. Lokey, J. H. McKerrow, K. Boundy-Mills, A. Nukanto, A. Kanti, H. Julistiono, L. B. S. Kardono, L. F. Bjeldanes and P. Crews, *J. Nat. Prod.*, 2011, **74**, 2545–2555.

3 G. M. Cragg and D. J. Newman, *Phytochem. Rev.*, 2009, **8**, 313–331.

4 G. M. Cragg, P. G. Grothaus and D. J. Newman, *Chem. Rev.*, 2009, **109**, 3012–3043.

5 M. Gordaliza, M. A. Castro, J. M. M. del Corral and A. San Feliciano, *Curr. Pharm. Des.*, 2000, **6**, 1811–1839.

6 C. Spatafora and C. Tringali, Phenolic oxidative coupling in the biomimetic synthesis of heterocyclic lignans, neolignans and related compounds, in *Targets in Heterocyclic Systems. Chemistry and Properties*, ed. D. S. O. Attanasi, Società Chimica Italiana, Roma, 2007, vol. 11, pp. 284–312.

7 C. Daquino, A. Rescifina, C. Spatafora and C. Tringali, *Eur. J. Org. Chem.*, 2009, 6289–6300.

8 (*a*) F. Mazue, D. Colin, J. Gobbo, M. Wegner, A. Rescifina, C. Spatafora, D. Fasseur, D. Delmas, P. Meunier, C. Tringali and N. Latruffe, *Eur. J. Med. Chem.*, 2010, **45**, 2972–2980; (*b*) G. Valdameri, L. P. Rangel, C. Spatafora, J. Guitton, C. Gauthier, O. Arnaud, A. Ferreira-Pereira, P. Falson, S. M. B. Winnischofer, M. E. M. Rocha, C. Tringali and A. Di Pietro, *ACS Chem. Biol.*, 2012, **7**, 321–329; (*c*) V. M. Bhusainahalli, C. Spatafora, M. Chalal, D. Vervandier-Fasseur, P. Meunier, N. Latruffe and C. Tringali, *Eur. J. Org. Chem.*, 2012, 5217–5224.

9 S. A. S. Silva, A. L. Souto, M. F. Agra, E. V. L. Cunha, J. M. Barbosa-Filho, M. S. Silva and R. Braz, *ARKIVOC*, 2004, 54–58.

10 S. Shi, Y. Zhang, K. Huang, S. Liu and Y. Zhao, *Food Chem.*, 2008, **108**, 402–406.

11 T. Tanaka, A. Nishimura, I. Kouno, G. Nonaka and C. R. Yang, *Chem. Pharm. Bull.*, 1997, **45**, 1596–1600.

12 Z. H. Jiang, T. Tanaka and I. Kouno, *Chem. Pharm. Bull.*, 1996, **44**, 1669–1675.

13 M. Kumar, P. Rawat, N. Rahuja, A. K. Srivastava and R. Maurya, *Phytochemistry*, 2009, **70**, 1448–1455.

14 M. A. E. Watanabe, M. K. Amarante, B. J. Conti and J. M. Sforcin, *J. Pharm. Pharmacol.*, 2011, **63**, 1378–1386.

15 S. Di Micco, F. Mazué, C. Daquino, C. Spatafora, D. Delmas, N. Latruffe, C. Tringali, R. Riccio and G. Bifulco, *Org. Biomol. Chem.*, 2011, **9**, 701–710.

16 G. Basini, L. Baioni, S. Bussolati, F. Grasselli, C. Daquino, C. Spatafora and C. Tringali, *Invest. New Drugs*, 2012, **30**, 186–190.

17 (*a*) V. Vijayakurup, C. Spatafora, C. Daquino, C. Tringali, P. Srinivas and S. Gopala, *Life Sci.*, 2012, **91**, 1336–1344; (*b*) V. Vijayakurup, C. Spatafora, C. Tringali, P. C. Jayakrishnan, P. Srinivas and S. Gopala, *Mol. Biol. Rep.*, 2014, **41**, 85–94.

18 C. Spatafora, C. Daquino, C. Tringali and R. Amorati, *Org. Biomol. Chem.*, 2013, **11**, 4291–4294.

19 (*a*) C. Hotzel, A. Marotto and U. Pindur, *Eur. J. Med. Chem.*, 2003, **38**, 189–197; (*b*) C. Keuser and U. Pindur, *Pharmazie*, 2006, **61**, 261–268; (*c*) M. H. David-Cordonnier, M. P. Hildebrand, B. Baldeyrou, A. Lansiaux, C. Keuser, K. Benzschawel, T. Lemster and U. Pindur, *Eur. J. Med. Chem.*, 2007, **42**, 752–771.

20 (*a*) C. Bourdouxhe Housiaux, P. Colson, C. Houssier, M. J. Waring and C. Bailly, *Biochemistry*, 1996, **35**, 4251–4264; (*b*) R. Zhang, X. Wu, L. J. Guziec, F. S. Guziec,

G. L. Chee, J. C. Yalowich and B. B. Hasinoff, *Bioorg. Med. Chem.*, 2010, **18**, 3974–3984; (*c*) U. Pindur, M. Jansen and T. Lemster, *Curr. Med. Chem.*, 2005, **12**, 2805–2847.

21 S. Di Micco, C. Bassarello, G. Bifulco, R. Riccio and L. Gomez-Paloma, *Angew. Chem., Int. Ed.*, 2006, **45**, 224–228.

22 (*a*) M. Mayer and B. Meyer, *Angew. Chem., Int. Ed.*, 1999, **38**, 1784–1788; (*b*) M. Mayer and B. Meyer, *J. Am. Chem. Soc.*, 2001, **123**, 6108–6117.

23 S. Grasso, L. Siracusa, C. Spatafora, M. Renis and C. Tringali, *Bioorg. Chem.*, 2007, **35**, 137–152.

24 I. Gomez-Monterrey, P. Campiglia, A. Carotenuto, D. Califano, C. Pisano, L. Vesci, T. Lama, A. Bertamino, M. Sala, A. Mazzella di Bosco, P. Grieco and E. Novellino, *J. Med. Chem.*, 2007, **50**, 1787–1798.

25 L. Martino, A. Virno, B. Pagano, A. Virgilio, S. Di Micco, A. Galeone, C. Giancola, G. Bifulco, L. Mayol and A. Randazzo, *J. Am. Chem. Soc.*, 2007, **129**, 16048–16056.

26 A. Leo, C. Hansch and D. Elkins, *Chem. Rev.*, 1971, **71**, 525–616.

27 (*a*) Y. Henchoz, D. Guillarme, S. Rudaz, J. L. Veuthey and P. A. Carrupt, *J. Med. Chem.*, 2008, **51**, 396–399; (*b*) C. Giaginis and A. Tsantili-Kakoulidou, *J. Liq. Chromatogr.*, 2008, **31**, 79–96.

28 (*a*) M. Calvani, L. Critelli, G. Gallo, F. Giorgi, G. Gramiccioli, M. Santaniello, N. Scafetta, M. O. Tinti and F. De Angelis, *J. Med. Chem.*, 1998, **41**, 2227–2233; (*b*) A. Drews, S. Bovens, K. Roebrock, C. Sunderkotter, D. Reinhardt, M. Schafers, A. van der Velde, A. S. Elfringhoff, J. Fabian and M. Lehr, *J. Med. Chem.*, 2010, **53**, 5165–5178; (*c*) J. Mun, A. A. Jabbar, N. S. Devi, S. M. Yin, Y. Z. Wang, C. Tan, D. Culver, J. P. Snyder, E. G. Van Meir and M. M. Goodman, *J. Med. Chem.*, 2012, **55**, 6738–6750.

29 M. C. Foti, C. Daquino and C. Geraci, *J. Org. Chem.*, 2004, **69**, 2309–2314.

30 B. Etzenhouser, C. Hansch, S. Kapur and C. D. Selassie, *Bioorg. Med. Chem.*, 2001, **9**, 199–209.

31 M. DellaGreca, L. Previtera, R. Purcaro and A. Zarrelli, *J. Nat. Prod.*, 2007, **70**, 1664–1667.

32 Y. Naito, M. Sugiura, Y. Yamaura, C. Fukaya, K. Yokoyama, Y. Nakagawa, T. Ikeda, M. Senda and T. Fujita, *Chem. Pharm. Bull.*, 1991, **39**, 1736–1745.

33 D. K. Kim, J. P. Lim, J. W. Kim, H. W. Park and J. S. Eun, *Arch. Pharmacal Res.*, 2005, **28**, 39–43.

34 J. Fu, K. Cheng, Z. M. Zhang, R. Q. Fang and H. L. Zhu, *Eur. J. Med. Chem.*, 2010, **45**, 2638–2643.

35 V. Sklenar, M. Piotto, R. Leppik and V. Saudek, *J. Magn. Reson.*, 1993, **102**, 241–245.

36 *MacroModel, version 8.5*, Schrodinger LLC, New York, NY, 2003.

37 (*a*) W. D. Cornell, P. Cieplak, C. I. Bayly, I. R. Gould, K. M. Merz, D. M. Ferguson, D. C. Spellmeyer, T. Fox, J. W. Caldwell and P. A. Kollman, *J. Am. Chem. Soc.*, 1995, **117**, 5179–5197; (*b*) S. J. Weiner, P. A. Kollman, D. A. Case, U. C. Singh, C. Ghio, G. Alagona, S. Profeta, Jr. and P. K. Weiner, *J. Am. Chem. Soc.*, 1984, **106**, 765–784; (*c*) P. A. K. S. J. Weiner, D. T. Nguyen and D. A. Case, *J. Comput. Chem.*, 1986, **7**, 230–252; (*d*) P. K. Weiner and P. A. Kollman, *J. Comput. Chem.*, 1981, **2**, 287–303.

38 W. C. Still, A. Tempczyk, R. C. Hawley and T. Hendrickson, *J. Am. Chem. Soc.*, 1990, **112**, 6127–6129.

39 T. A. Halgren, *J. Comput. Chem.*, 1996, **17**, 616–641.

40 R. Huey, G. M. Morris, A. J. Olson and D. S. Goodsell, *J. Comput. Chem.*, 2007, **28**, 1145–1152.